UNIVERSITY OF CALIFORNIA SAN DIEGO

Multiscale Approach Towards the Development and Usage of Electrochemical Energy Storage

A dissertation submitted in partial satisfaction of the
requirements for the degree Doctor of Philosophy

in

NanoEngineering

by

Daniel Davies

Committee in charge:

Professor Ying Shirley Meng, Chair
Professor Graham Elliot
Professor David Fenning
Professor Jan Kleisl
Professor Ping Liu

2020

The Dissertation of Daniel Davies is approved, and it is acceptable in quality and form for publication on microfilm and electronically:

_____

_____

_____

_____

_____

Chair

University of California San Diego
2020

DEDICATION

To my brother: Luke

TABLE OF CONTENTS

LIST OF FIGURES

LIST OF TABLES

ACKNOWLEDGEMENTS

I would like to thank my family for their incredible support throughout this process.

Next, I would like to thank my San Diego friends for all their support! Especially Lingy, Ashish, Anna, Lennart, and Tom for their great support and for making my time in San Diego fun when I wasn't working!

I would like to express my deepest gratitude to Emma and her family for their unending support, especially throughout 2020 when I was juggling writing my paper and thesis with my internship – all during the Covid Pandemic. Emma really carried me through some trying times and provided such a loving and supportive environment

I am incredibly appreciative of the opportunities that Shirley has provided me throughout my Ph.D. Her flexibility has allowed me to pursue my interests unabatedly. She supported me working through an economics project, transitioning through mechanical design, and finally moving back towards computation. During this, she also encouraged me to pursue a Micro-MBA through the Rady school and then even helped me to secure an internship at Tesla during 2020. Her guidance and motivation have been absolutely crucial to my Ph.D. experience.

I want to give special mention to Cyrus who helped me immensely both as a friend and scientist throughout this whole experience. His passion and dedication for science were incredibly inspiring and motivating, and I owe so much of my career to his great mentorship. I truly hope that we are able to work (and surf) together soon in the future.

To the LGE subgroup – Yang, Jackie, Katya, and Matt, you have been an absolute joy to work with. I'm so glad that we were able to keep our little hideaway lab safe and productive throughout all of these years. Thank you so much for your help and scientific discussions over the years.

I would also like to give special mention to Oleg Borodin. Your guidance, mentorship and support throughout my last few years has been tremendous. You have been tremendously generous with your advice and time and have really revolutionized our understanding of the liquefied gas electrolytes. I hope that the LGE group has the pleasure of continuing to work with you in the future.

I would also like to thank Graham Elliot for his help and guidance during the CHARGES project. I am very appreciative of your patient explanations, and especially the guidance you gave me in scientific writing. Also, to Rohan who was my first undergraduate mentee on the CHARGES project. I am incredibly appreciative of your patience and willingness to work. The paper wouldn't have been a success without your incredible help.

I also would like to acknowledge and thank my collaborators and co-authors at UC San Diego: Dr. Thomas Wynn, Dr. Marco Olguin, Dr. Dijo Damien, Dr. Michael Verde, Dr. Jungwoo Lee, Dr. Pritesh Parikh, Dr. Jean-Marie Doux, Dr. Abhik Banerjee, Darren H.S. Tan, Diyi Cheng, Yihui Zhang, Bingyu Lu, Oleksiy Mynshenko, Ying Ru Chen, Dr. Antonio Tong, and Bill Torre.

I have learned so much from all the members of the Laboratory for Energy Storage and Conversion group (past and present) and it has been a pleasure working with them.

Finally, I would like to thank my funding sources: The Advanced Research Projects Agency–Energy (ARPA-E) the U.S. Department of Energy under award number DE-AR000520 as part of the Cycling Hardware to Analyze and Ready Grid-Scale Electricity Storage (CHARGES) program. South 8 Technologies under National Science Foundation NSF SBIR program (Grant No. 1721646 and 1831087).

Chapter 4, in full, is a reprint of the material "Combined Economic and Technological

Evaluation of Battery Energy Storage for Grid Applications" as it appears in Nature Energy, D. M. Davies, M. G. Verde, O. Mnyshenko, Y. R. Chen, R. Rajeev, Y. S. Meng & G. Elliott. The dissertation author was the primary investigator and first author of this paper.

Chapter 5, in full, is a reprint of the patent application "Electrochemical Cell Cap for Liquefied Gas Electrolyte" as it appears in US Patent App. 16/666,131, C.S. Rustomji, Y. Yang, D. M. Davies, J. Lee, Y.S. Meng. The dissertation author was primary investigator and first author of the patent application.

Chapter 6, in full, is a reprint of the material "A Safer, Wide Temperature Liquefied Gas Electrolyte Based on Difluoromethane" by D. M. Davies, Y. Yang, E. S. Sablina, Y. Yin, M. Mayer, Y. Zhang, M. Olguin, J. Z. Lee, B. Lu, D. Damien, O. Borodin, C. S. Rustomji, and Y. S. Meng which is under review at Journal of Power Sources

VITA

2014 Bachelor of Mechanical and Aerospace Engineering

Princeton University

2016 Master of Science in NanoEngineering

University of California San Diego

2020 Doctor of Philosophy in NanoEngineering

University of California San Diego

PUBLICATIONS

Davies, D. M., Verde, M. G., Mnyshenko, O., Chen, Y. R., Rajeev, R., Meng, Y. S., & Elliott, G. (2019). Combined economic and technological evaluation of battery energy storage for grid applications. *Nature Energy*, *4*(1), 42–50. https://doi.org/10.1038/s41560-018-0290-1

Davies, D.M., Rustomji, C. S., Yang, Y., Lee, J., & Meng, Y. S. (2020, February 27). *Electrochemical cell cap*. US Patent App. 16/666,155.

Rustomji, C. S., Yang, Y., **Davies, D.M.**, Lee, J., & Meng, Y. S. (2020, February 27). *Chemical formulations for electrochemical device*. US Patent App. 16/666,131.

Davies, D. M., Yang, Y., Sablina, E.S., Yin Y., Mayer, M., Zhang Y., Olguin, M., Lee, J.Z., Lu, B., Damien, D., Borodin, O., Rustomji, C.S., and Meng, Y.S. (Under Review). A Safer Wide-Temperature Liqueified Gas Electrolyte Based on Difluoromethane. *Journal of Power Sources.*

Yang, Y., **Davies, D. M.**, Yin Y., Borodin, O., Lee, J.Z., Fang, C., Olguin, M., Wang, X., Zhang Y, Sablina, E.S., Cyrus . Rustomji, C.S., and Meng, Y.S. (2019). High Efficiency Lithium Metal Anode Enabled by Liquefied Gas Electrolytes. *Joule*.

Yang, Y., Yin, Y., **Davies, D. M.**, Zhang, M., Mayer, M., Zhang, Y., … Meng, Y. S. (2020). Liquefied gas electrolytes for wide-temperature lithium metal batteries. *Energy & Environmental Science*, *13*(7), 2209. https://doi.org/10.1039/d0ee01446j

Wynn, T. A., Fang, C., Zhang, M., Liu, H., **Davies, D. M.**, Lau, D., Zee, J.L., Huang, B.Y., Wang, X., Fung, K.N., Ni, C.T., and Meng, Y. S. (2018). Mitigating oxygen release in anionic-redox-active cathode materials by cationic substitution through rational design. *Journal of Materials Chemistry A*, *6*(47), 24651–24659. https://doi.org/10.1039/c8ta06296j

Root, S. E., Carpenter, C. W., Kayser, L. V., Rodriquez, D., **Davies, D. M.**, Wang, S., … Lipomi, D. J. (2018). Ionotactile Stimulation: Nonvolatile Ionic Gels for Human-Machine Interfaces. *ACS Omega*, *3*(1), 662–666. https://doi.org/10.1021/acsomega.7b01773

Keef, C. V., Kayser, L. V., Tronboll, S., Carpenter, C. W., Root, N. B., Finn, M., **Davies, D.M.** … Lipomi, D. J. (2020). Virtual Texture Generated Using Elastomeric Conductive Block Copolymer in a Wireless Multimodal Haptic Glove. *Advanced Intelligent Systems*, *2*(4), 2000018. https://doi.org/10.1002/aisy.202000018

ABSTRACT OF THE DISSERTATION

Multiscale Approach Towards the development and usage of electrochemical energy storage

by

Daniel M. Davies

Doctor of Philosophy in NanoEngineering

University of California San Diego, 2020

Professor Ying Shirley Meng, Chair

Batteries are a crucial component in the transition to renewable energy required to combat catastrophic climate change. The development of rechargeable batteries is a multi-scale issue requiring understanding and innovation from atomistic material science all the way through international infrastructure and financial modeling. At each scale of development, multi-faceted approaches to design and innovation are required, ranging from quantum mechanical modeling through electrochemical and mechanical engineering to economic analyses.

In this thesis, a top-down approach is used, exploring economics of large-scale batteries

for grid use, moving through mechanical design of housing for battery cells using novel electrolytes, and finally electrochemical design and molecular level characterization of these novel electrolytes. At the grid scale, models of storage connected to the California energy grid are used to show how the duty-cycles (power profiles) of different applications affect different battery chemistries. Critical tradeoffs between battery chemistries, energy applicability and revenue generation in various markets on the California grid are revealed. Accurate revenue measurement can only be achieved if realistic battery operation in each application is considered. At the cell scale, methods, systems and devices are described for implementing electrochemical energy storage devices using novel liquefied gas solvents in the conventional and manufacturable 18650 form-factor for next-generation Li-metal batteries and beyond. An enhanced safety feature inherent in liquefied gas electrolytes is also demonstrated. Finally, at the molecular scale, the viability of using difluoromethane as the primary liquefied gas solvent which has lower pressure, lower flammability and improved maximum temperature operation characteristics. The multi-scale approach used in this dissertation provides insight and understanding to a range of battery storage technologies and helps to lower the risk of adoption of a novel class of electrolytes for next-generation batteries.

Chapter 1. Motivation and Outline

1.1 Introduction and a Multi-Scale Approach

In 2019, the overall global primary energy usage was over 140,000 TWh[1]. With the vast majority coming from fossil-fuel based sources (oil, coal and gas). Burning of these fuels has released a huge amount of Carbon Dioxide, a greenhouse gas, into the atmosphere. This significant increase in emissions has led to a dangerous rise in the atmospheric carbon dioxide levels, causing global warming and other global-scale climate disasters[1].

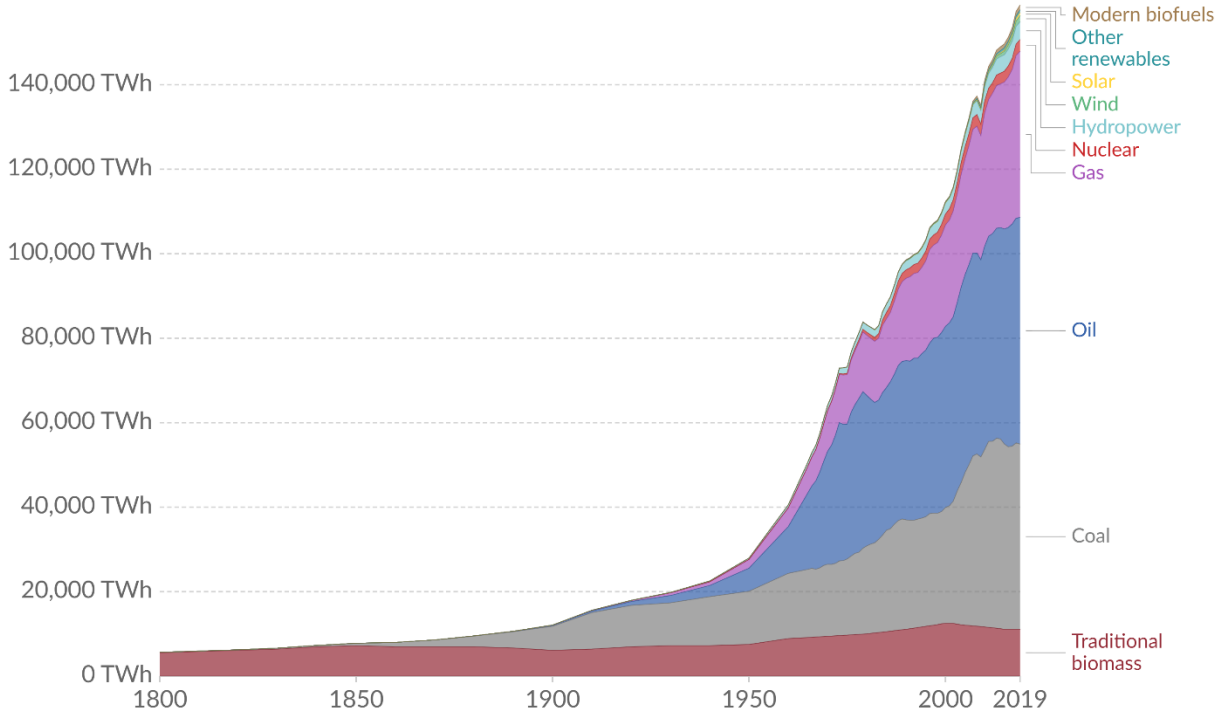

Figure 1.1 Global Primary Energy Usage[2]

It has been estimated that restricting the overall temperature rise of the earth to less that of 1.5 ℃ by 2050 will limit the number of people susceptible to climate-related poverty by several hundred million[3]. In order to achieve this goal, if emissions were to peak today, we would need to reduce emissions by 15% each year. The longer the world waits to substantially

reduce emissions, the more dramatic the change will need to be.

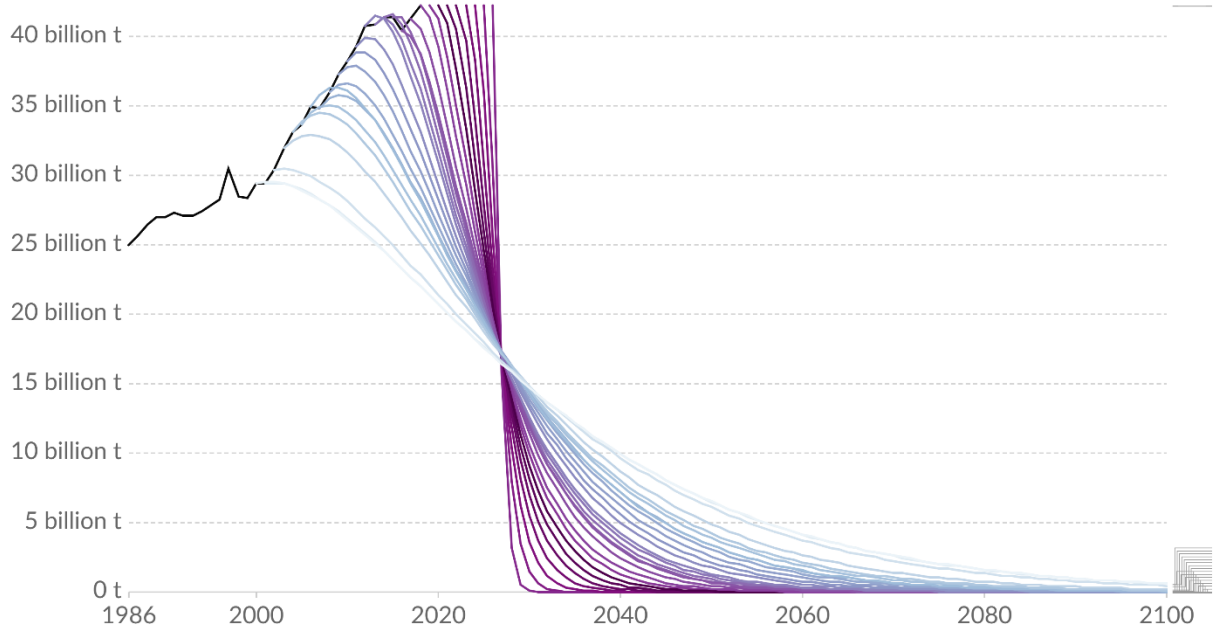

Figure 1.2 Emissions of carbon dioxide per year required to keep global average temperature rise below 1.5 ℃. Scenarios are based on the reduction needed with different global peaks in emission[2].

In order to achieve this, it is crucial that carbon-free energy generation becomes the dominant mechanism for producing energy world-wide. Future growth in energy usage is expected to be dominated by the transportation sector and the electrical grid, and therefore, these areas are crucial to decarbonize. This is a complex endeavor, arguably of which the most challenging part is the energy storage required to make this transition. Energy storage becomes increasingly crucial as more carbon-free, renewable sources are used. For grid-scale applications, the reliability of the systems depends on storage to make up for the intermittent nature of renewable energy generation sources, while in the transportation industry, the energy needs to be portable and so storage must be used. For both applications, electrochemical-energy storage in form of batteries is a key player.

The global battery market in 2019 was estimated to be worth $108.4 billion, with an expected market size of over $300 billion in 2027[4]. Over the many decades of intense

development[6], a large number of chemistries and form-factors have been formulated and used for a vast number of applications ranging small-scale portable electronics all the way through grid-scale energy storage. Historically, lead-acid batteries have found success in car ignition batteries, and larger scale, high power batteries for power banks. Nickel-based batteries had found success in power tools, drones and vehicles due to their relatively high energy density. Li-ion batteries have been used for space and weight constrained products such as portable electronics, and more recently, electric vehicles. Additionally, primary (single charge) batteries have been used in many applications ranging from medical devices to aerospace. Figure 1.3 gives an overview of the U.S. battery market size for common rechargeable batteries.

Both the importance of the problem as well as the complexity of the battery industry are immense. When looking to develop batteries, there are a number of facets that need to be considered, stemming all the way from the economics of how batteries are used in markets, all the way down to what atoms are undergoing the necessary Redox reactions provide the energy for these applications.

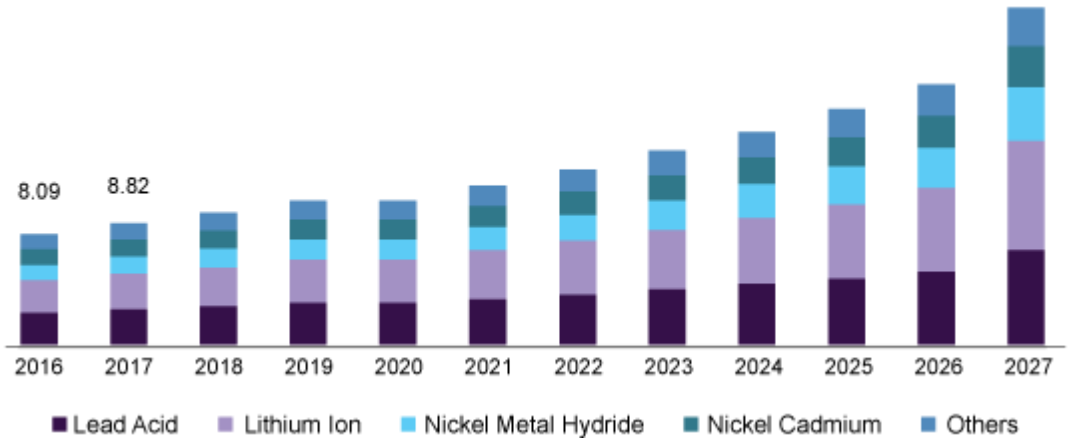

Figure 1.3 U.S. Battery market size, 2016-2027 (USD Billion)[5]

1.2 Grid Scale Storage

Renewable energy sources, such as wind and solar, are inherently intermittent and for this reason, they will be unable to provide 100% of the grid-scale energy without the use of energy storage. As a clear example, the amount of energy generated by solar panels fluctuates rapidly with cloud cover. Figure 1.4 shows the famous "duck curve" of the California Grid. The curve illustrates a large overgeneration risk in the middle of the day when the demand for energy is relatively smaller, and the energy generated by renewable sources is relatively higher.

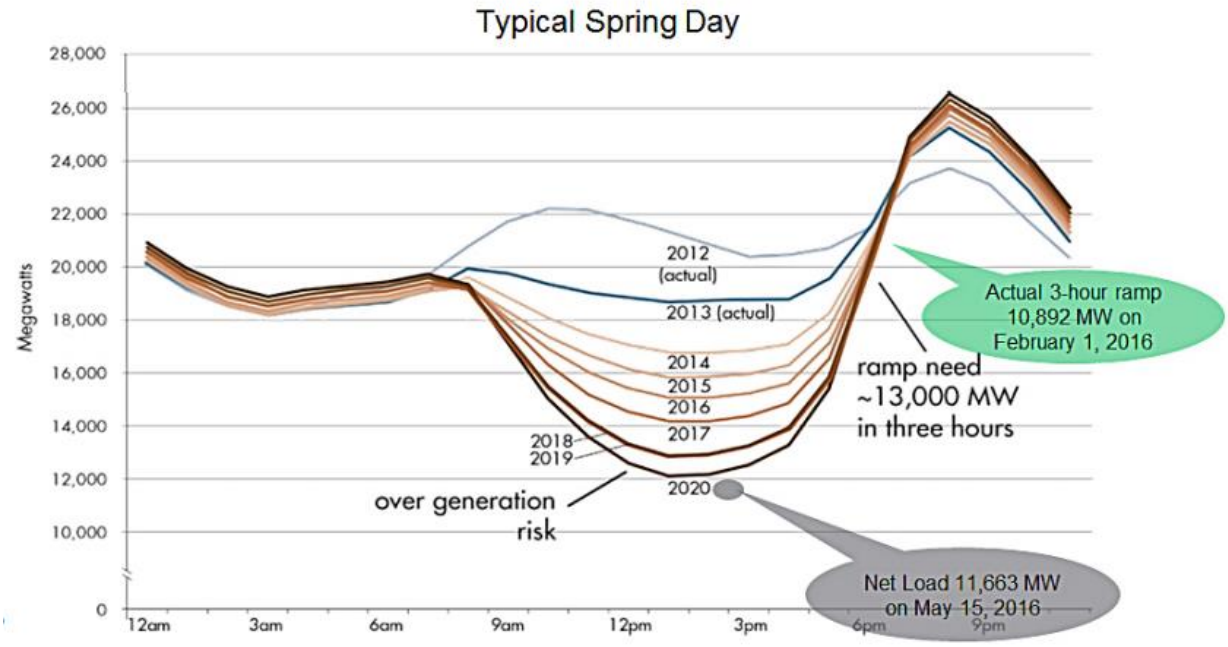

Figure 1.4 The "Duck Curve" showing the energy load minus the renewable generation on the California Grid on a typical spring day. [6]

Moreover, there are a number of other services that energy storage can provide to the electrical grid – especially as the "flexibility" and response time of the energy storage increases. These include applications such as frequency regulation, load management, and uninterruptable power supplies. Energy storage technology may be more suitable for one application than another. For example, hydro-electric storage is well suited for applications involving large shifts

of energy over a long period (hours), however, due to the long lag time required to ramp power output, this large storage would not perform well in the frequency regulation application which requires power fluctuations on the order of seconds. Understanding these applications and the requirements for grid-connected storage to perform these duties is an evolving and challenging process.

Batteries are an attractive option for grid-scale energy storage due to their power flexibility (relatively fast ramp time when compared with other storage options), and their scalability. Historically, push for energy density for batteries used in grid scale applications has been relatively small – with larger emphasis historically being placed on the cost and the cycle life of the batteries[7]. However, as the cost of batteries decrease, and the demand and number of applications for grid storage increases, many different chemistries are being explored for potential use in on the grid. These include, but are not limited to Li-ion chemistries, lead-acid, aqueous flow batteries, vanadium flow batteries and sodium-based chemistries.

As the grid-scale applications and the energy storage technologies rapidly evolve, both thorough economic and technological understanding of the systems is required to understand their relationships in order to select and design the optimal storage solutions for the grid.

1.3 Transportation, High Energy Density Batteries

For transportation applications, Nickel-based chemistries, and especially Li-ion-based batteries have proved effective due to their relatively large energy densities. However, to increase the adoption of electrical vehicles (and other electric based transportation) there is still demand for higher energy density. As researchers and manufacturers are nearing the theoretical limits of current graphite-based Li-ion chemistries, the scientific community is looking to Li-metal to replace graphite as the anode. Li-metal boasts a much higher theoretical capacity than graphite

and is also a source of Li, thus enabling the use of promising cathode chemistries such as Sulfur or Oxygen. Its adoption has been limited, however, due to low coulombic efficiency and large relative volume growth. The development of new electrolytes has proved to be one of the more promising pathways forward to enabling the adoption of Li-metal batteries.

Recently, there have been developments in electrolyte systems that make use of solvents that are gaseous at room temperature and pressure. At moderate pressures or low temperatures, these molecules can be liquified and function as solvents that are able to dissolve Li salts – creating liquified gas electrolytes. The low melting point low viscosity, inherent pressure, electrochemical stability and high donatable fluorine content combine synergistically to enable excellent performance in Li-metal based batteries, even down to temperatures as low as -60 ℃. There has, however, been concerns about the practicality and manufacturability of electrochemical storage devices utilizing these liquefied gas solvents. These concerns are mainly centered around the inherent pressure, flammability, and low critical temperature of fluoromethane.

Previous work in our group has focused mainly on using fluoromethane as the liquefied gas electrolyte, cycled in large stainless-steel vessels in order to safely hold the pressure. For technology to become widely adopted, it needs to be mass producible. The likelihood of adoption is far greater as well if the technology is able to easily be adapted into existing manufacturing lines. The form factors selected for use with liquefied gas electrolytes need to be compatible with the moderate pressures associated with the solvents. In order to reduce the amount of non-energy contributing mass it is best to use a cylindrical form factor to hold the moderate pressures of the electrolytes. Cylindrical Li-ion form-factors are typically either 18650 (18 mm diameter, 65 mm length), or 21700 (21 mm diameter, 70 mm length). Typically, the filling of the electrolyte in the

manufacturing process constitutes its own step. A great solution for lowering the barriers to adoption would be to only impact this filling step – i.e. providing a "drop-in" replacement solution for existing manufacturing lines.

As with any new technology there are also barriers to adoption outside of the manufacturability. One of the areas of most concern is the safety of the electrolyte. The primary concern associated with Li-ion batteries is thermal runaway of cells. The fluoromethane based electrolyte, like conventional liquid electrolytes is flammable. Due to its pressurized nature there has been additional concern about this. There is, however, possibility that the nature of the liquefied gas electrolytes may help to suppress the possibility of thermal runaway. Pressurized electrolytes may allow venting and thereby rapid cooling of cells by the ideal gas law.

$$PV = nRT$$

Additional ways to reduce the flammability of the electrolytes and increase the maximum operation temperature should also be explored to help to lower the barriers of adoption of this novel electrolyte system for the advancement of high-energy density batteries.

My Ph.D. thesis consists of 7 chapters. Including this motivation (**Chapter 1**). **Chapter 2** provides a general introduction to the working principles of batteries and electrolytes. **Chapter 3** briefly introduces the advanced characterization tools that I applied in my research including Raman and Molecular Dynamics (MD) simulations. **Chapter 4** presents a technological and economic analysis of battery storage connected to the California grid. **Chapter 5** describes the invention of methods and apparatuses to fill and contain liquefied gas electrolytes in conventional form-factor 18650 electrochemical cells. **Chapter 6** presents a safety feature inherent to liqueified gas electrolytes and demonstrates the molecular design, and viability, of using a less flammable molecule as the primary liquefied gas solvent. **Chapter 7** summaries the

work and discusses ideas for future research.

Chapter 2 Working Principles of (Li-ion) Batteries and Electrolytes

There are various battery chemistries explored in this thesis. For simplicity, the working principles of batteries are explained by examining the mechanisms of the Li-ion battery – many of the concepts can be generalized, although significant differences in the mechanisms do exist between chemistries. In general, batteries consist of an anode (with a current collector), a cathode (with a current collector), and a separator. All components are soaked in an electrolyte. An electrical circuit is created by allowing the ions to flow between the electrodes through the electrolyte (and separator), while electrons are directed through an external circuit.

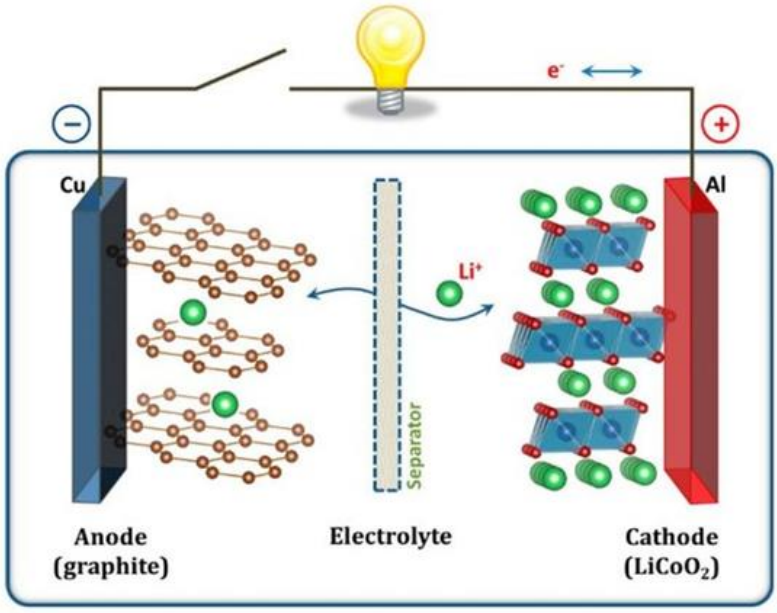

Figure 2.1 – Working principle of the Li-ion battery[8]

The electrochemical energy stored by a battery is the result of the Voltage difference between the two electrodes, as well as the capacity of the electrodes (in the case of Li-ion batteries, this is the number of Li ions that the electrodes are able to repeatably store). Cathode materials are conventionally layered oxide materials with the formula $LiMO_2$ where M represents particular transition metals. Since their invention in 1991[9], graphite has been the dominant anode material, with Li-ions being able to intercalate in between the layers of carbon.

Electrolytes are typically Li-based salts dissolved in organic solvents.

The Voltage difference between the two electrodes is based on the chemical potential difference between the two electrodes. This potential difference can be thought of as the driving force of the battery. During discharge, the Li ions de-intercalate from the graphite anode, and are pushed into the cathode material. In order to maintain charge neutrality, electrons are forced through the external circuit where they can perform useful work. During the charging process, the external circuit drives the electrons in the opposite direction. In order to maintain charge neutrality, the Li ions are forced from the cathode material back into the anode material. In the case of Li-ion batteries, the Li always stays in its ionic form and is intercalated and de-intercalated from both the anode and cathode in what is known as a “rocking chair” motion. In many other battery chemistries, the active ions undergo chemical reactions at one, or both electrodes. These “conversion” reactions are common in many chemistries including lead, or nickel-based batteries.

2.1 The role and brief history of electrolytes

The electrolyte in Li based batteries serves to transport Li ions between the electrodes while preventing the transport of electrons through the separator. Historically, they have consisted of Li-based salts dissolved in a supporting medium, for example, an organic-based liquid. As their primary job is to move ions, there are some qualities that need to be present in electrolytes for them to be effective in batteries including high ionic conductivity, low electronic conductivity, safety, low toxicity, and low cost.

One of the primary challenges associated with designing and selecting electrolytes for Li-based batteries is the wide electrochemical window required to prevent sides reactions at the

electrodes of the battery. This electrochemical window is defined by the lowest unoccupied molecular orbital (LUMO) and the highest occupied molecular orbital (HOMO). This is demonstrated in Figure 2.2a where it is seen that the electrolyte will be reduced by an anode with a potential above the LUMO and oxidized by a cathode with a potential below the HOMO. Figure 2.2b shows that although the electrolytic window of commercialized carbonate electrolytes envelopes many of the cathode chemistries used today, graphite and Li-metal fall outside this window and so reduction of the electrolyte is expected at these anodes. The key to the success of the commercialization of graphite-based Li-ion batteries is the solid-electrolyte interface that develops between the carbonate-based electrolytes and the graphite anode known as the SEI. This passivating SEI layer allows the continued operation of the batteries even outside of the electrolytic window.

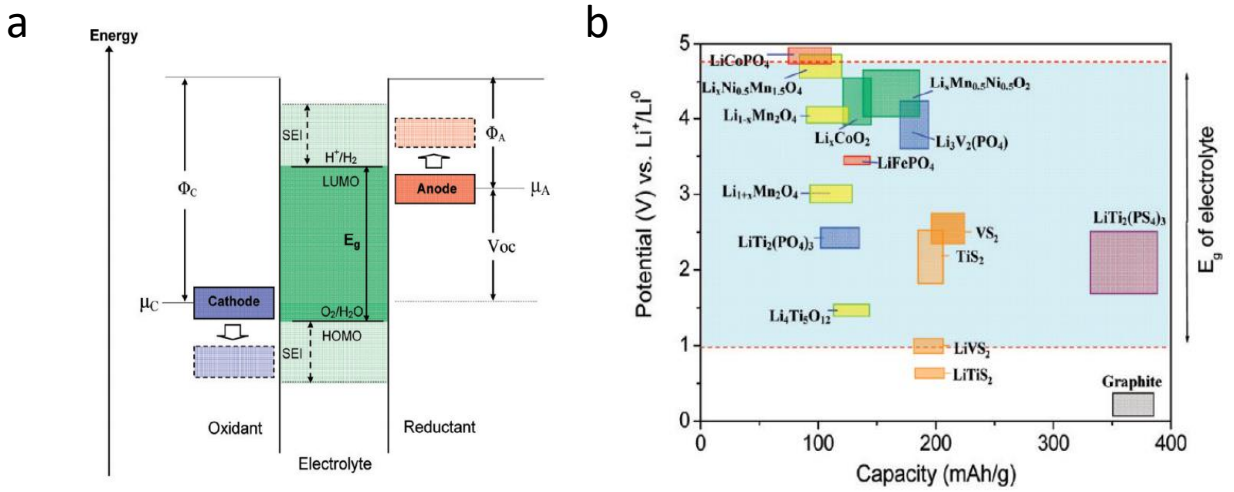

Figure 2.2 Li based batteries electrolytic window. (a) Illustration energy diagram Li-ion batteries (b) Voltage and capacity of many electrodes for Li-ion batteries with the electrolytic window of conventional carbonate-based liquid electrolytes[10]

Since the commercialization of Li-ion batteries, the electrolyte has received relatively little attention. However, as the push towards new electrode chemistries intensifies, the research

community is seeing much more development of novel electrolytes. Especially in the case of the Li-metal anode, one of the primary challenges of electrolyte development is to find materials that create good interfaces with Li-metal that at the same time possess the necessary qualities of effective electrolytes – namely charge transport properties and compatibility with the cathode chemistries used.

Conventional carbonate-based electrolytes display poor compatibility with the Li-metal anode[11]. Liquid ether-based electrolytes have received attention due to the relatively good interfaces formed with Li-metal, however, these electrolytes suffer from low oxidation stability[12]. More recently, new types of electrolytes have been developed. “Solvent-in-salt” or high concentrated electrolytes have had success in forming stable SEIs through salt decomposition. However, there are a few drawbacks with these electrolytes due to their cost, viscosity, wettability, and inadequate performance at low temperatures. Further advances in this field have also brough about locally high concentrated electrolytes which have partially mitigated some of these disadvantages[13]. Importantly, the field has also begun to branch away from the traditional liquid-based electrolytes and a significant amount of effort has been put into solid-state electrolytes. These have been heralded for their potential safety enhancements; however, their usage has been hindered by low conductivity at ambient and low temperature[14]. As the community pushes towards higher and higher energy densities, electrolyte development becomes a more critical factor in the overall progress of next-generation batteries.

Chapter 3. Characterization Methods

3.1 Raman Spectroscopy

Raman spectroscopy is concerned with the measurement of the inelastic scattering of light from matter. This scattering was first postulated by Smekal in 1923, and was first observed experimentally by Raman and Krishnan in 1928[15]. In this experiment focused light was shone onto a sample, and the altered frequency from the incident was measured through a system of optical fibers and lenses.

When light strikes matter, a few things can happen. The photons either do no interact, are absorbed, or are scattered. The scattering of light is the basis of the Raman technique. The photon interacts with the sample and polarizes the electron cloud to form a “virtual-state”. This state is not stable, and the photon is quickly re-emitted. The most common form of scattering is elastic scattering, where the re-emitted photon has the same energy as the incident radiation, known as Rayleigh scattering[16]. If the vibrational state which the molecule returns to after passing through its virtual state is different from before the photon interacted with it, radiation will be emitted with a slightly different frequency, this is known as inelastic scattering. If the frequency of the emitted light is lower than that of the incident light this is known as Stokes scattering, if it is higher, it is known as anti-Stokes scattering. Figure 3.1 gives a visual depiction of the three types of scattering.

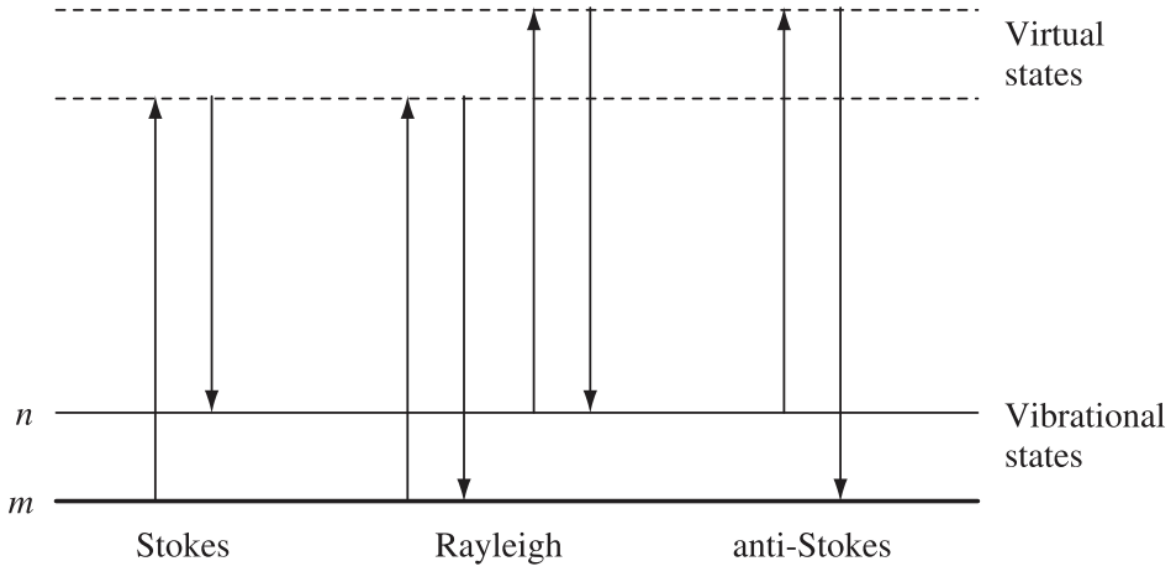

Figure 3.1 – Three types of scattering upon interaction of photons with molecules. Stokes and anti-Stokes transitions are examples of inelastic scattering, Rayleigh scattering is elastic. The lowest energy vibration state is shown as *m.* [16]

In practice, a single frequency of radiation is shone onto the sample, and radiation scattered from the sample is detected. Only 1 in about 10^6 to 10^8 photons are inelastically scattered, and so the Rayleigh frequency must be filtered out of the measurement or it overwhelms the results. It is also important to note that because the virtual states aren't stable states. Their energy is determined by the frequency of the light source whereas the vibrational states are dependent on the molecule and its local environment. This means that Raman spectra for molecules are somewhat independent of the frequency of light used to excite them.

Intense scattering is caused by vibrations which cause a change in the polarizability of the molecule, and symmetric vibrations cause the largest changes. The frequency shown in Raman plots is the result of the measured frequency subtracted from the frequency of the incident light. The intensity of the light emitted each frequency delta is then plotted. An example for Dichloromethane is shown in Figure 3.2.

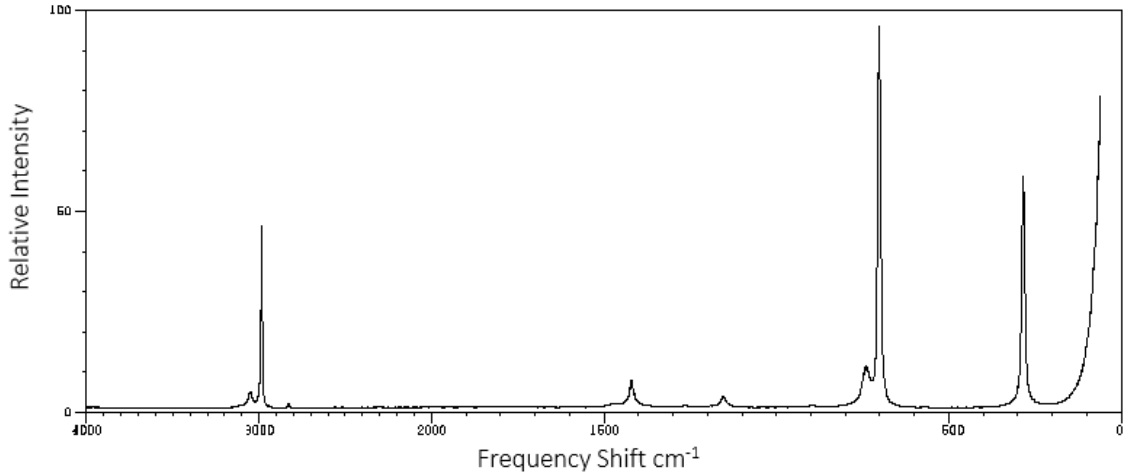

Figure 3.2 Example Raman spectra of dichloromethane[17]

Group theory is frequently used to help assign intensity peaks at certain frequencies to vibrations. For simplicity, I will not discuss this important aspect of spectra interpretation here. As the molecules get larger and more complex, assigning peaks to individual vibrations becomes more challenging and a common approach is to break down the problem into characteristic features. What is commonly done in research currently is to make use of the vast libraries of information about vibrational spectra to assign peaks seen in spectra to specific vibrations.

One of the most important aspects about vibrational spectroscopy is that the vibrational states of molecules and their bonds can vary significantly in different chemical environments. As an example, the characteristic vibration of the C≡N bond in Acetonitrile has characteristic frequency of 2254 cm^{-1}. However, when Nitrogen is coordinated to a cation such as Li^{+}, the characteristic frequency shift increases to 2277 cm^{-1} [18]. If the components of a solution or electrolyte are known, information can be gathered about the chemical environments of the constituents and even properties such as solvation structures of ions can be deduced.

3.1.1 Raman Spectroscopy of Liquefied Gas Electrolytes

The Raman spectroscopy of liquids is often performed in glass vials. When working with liquefied gas electrolytes, there is an additional complication due to the moderate pressures involved. Previous measurements of high-pressure systems (even explosive reactions) have previously successfully been taken, however, the apparatuses used were often custom and prohibitively expensive for our systems[19]. Additionally, as I was interested in trying to find the chemical environments of molecules that made up only a small percentage of the volume of electrolyte, it was important to design a device capable of holding a relatively large amount of liquid in order to boost the signal to noise ratio of measured electrolyte. This required a new design that was both chemically and mechanically compatible with all the components of the liquefied gas electrolytes being explored.

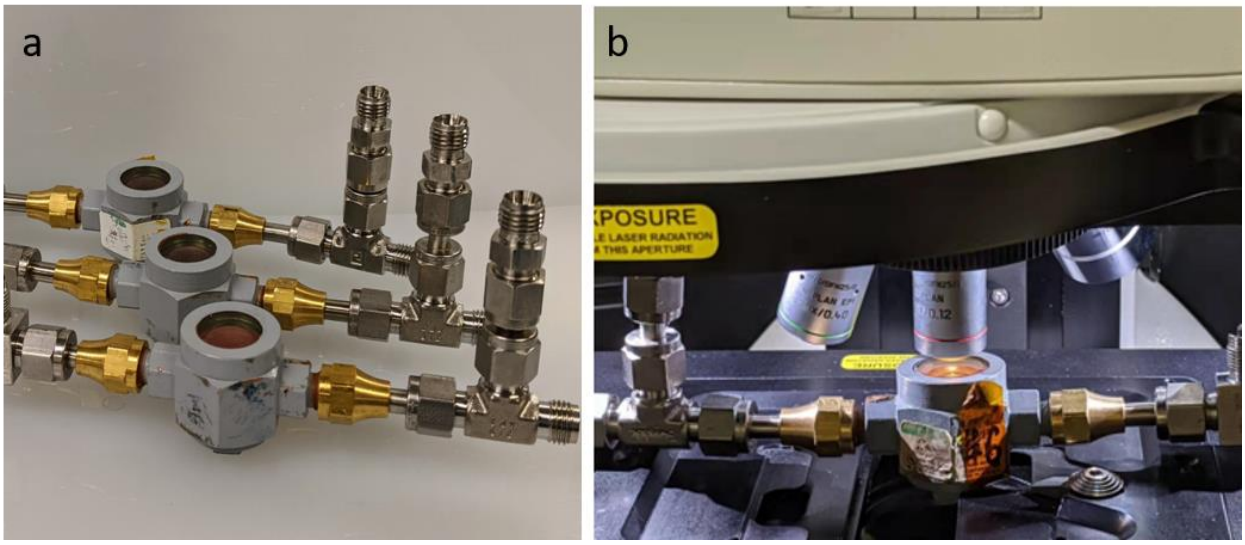

Figure 3.3 – Custom designed Raman setup. (a) 3 devices. (b) Device underneath the Raman microscope

The device (Figure 3.2), leveraged and adapted parts used in the refrigeration industry. The devices were rated up to 650 PSI, and thorough vetting of chemical and mechanical compatibility was conducted before use for the Raman measurements.

3.1.2 Molecular Dynamics Simulations

Molecular dynamics simulations are a tool used to aid in the understanding of systems. In principle, they take estimations of the interactions between molecules and use these to obtain predictions of bulk properties of systems. Often thought of as "bridge" between theory and experiment, these simulations allow researchers to test theories and models of microscopic behavior of systems. The bulk properties predicted by the models can be compared to experimental results which enables (at least partial) validation of theory and models developed. If accurate estimations of interactions between atoms and molecules are made, understanding of how these interactions relate on the microscopic scale to result in bulk properties can be obtained. This is also especially helpful for understanding of systems that are difficult (or impossible) to reach experimentally due to high pressures or temperatures. [20]

The basis of molecular dynamics is obtaining a numerical step-by-step solution of classical equations of motions.

$$\boldsymbol{f}_i = m_i \ddot{\boldsymbol{r}}_i$$

$$\boldsymbol{f}_i = \frac{\partial}{\partial \boldsymbol{r}_i} U$$

The forces $\boldsymbol{f}_i$ acting on the atoms are derived from the potential energy function

$$U(\boldsymbol{r}^N)$$

Where $\boldsymbol{r}^N$ represents the set of 3N atomic coordinates. Defining this potential energy is one of the main challenges associated with molecular dynamics simulations. The most common approach is to define a potential function and then use both empirical and first-principles data to parameterize these functions.

In classical molecular dynamics, the potential function is the sum of the non-bonded

interactions, and the bonded interactions as shown below:

$$U = U^{NonBonded} + U^{Bonded}$$

The nonbonded interactions are often defined as the sum of the repulsion and dispersion energy and the Coulombic Potential

$$U^{NonBonded} = U^{ReplusionDispersion} + U^{Coulombic}$$

$$U^{ReplusionDispersion} = 4\varepsilon\left[\left(\frac{\sigma}{r}\right)^{12} - \left(\frac{\sigma}{r}\right)^{6}\right]$$

$$U^{Coulombic} = \frac{Q_1 Q_2}{4\pi\epsilon_0 r}$$

Where σ, the diameter, ε, the well depth, and Q_1, Q_2, the charges are the variables that require parameterization.

The bonded interactions are often defined as the sum of the bonds, bends, torsion and dihedrals as shown below

$$U^{Bonded} = U^{Bond} + U^{Bend} + U^{Torsion}$$

$$U^{Bond} = \frac{1}{2}\sum_{Bonds} k_{ij}^{r}\left(r_{ij} - r_{eq}\right)^2$$

$$U^{Bend} = \frac{1}{2}\sum_{Bends} k_{ijk}^{\theta}\left(\theta_{ijk} - \theta_{eq}\right)^2$$

$$U^{Torsion} = \frac{1}{2}\sum_{Torsions}\sum_{m} k_{ijkl}^{\emptyset,m}\left(1 + \cos\left(m\emptyset_{ijkl} - \gamma_m\right)\right)^2$$

Where k_{ij}^{r}, r_{eq}, k_{ijk}^{θ}, θ_{eq}, $k_{ijkl}^{\emptyset,m}$, γ_m are the variables that require parameterization.

The combination of the function and the parameterization of the variables are known as the "force-fields" of the system. There has been a large amount of effort in the community to derive the most accurate forcefields for molecules. One of the main challenges in developing the models is to balance the tradeoff between accuracy (usually requiring more complicated models)

and computational efficiency. Approaches to parameterize models have used both first-principles calculations as well as empirical methods to determine the most accurate parameterizations.

Once the force-field is defined, an algorithm must be used to integrate Newton's equations of motion for all the particles in the simulation system simultaneously. Typically, this can be on the order of hundreds to millions of particles, and simulation types typically run from a few pico seconds to hundreds of nano seconds. The used algorithm must therefore be efficient and accurate.

The user must also select which "ensemble" they wish to use. The natural ensemble for Molecular Dynamics is the microcanonical ensemble NVE where the number of particles, volume and energy are kept consistent. Simulations are often performed that replicate as best as possible the experimental setup such as NPT (number of particles, pressure and temperature are held constant), and NVT (number of particles, volume and temperature are held constant).[20]

Finally, an experimental system may contain a huge number of particles $N_A = 6.02 \cdot 10^{23}$ molecules. A typical simulation contains 10^6 molecules. This means that in the simulation box, many of the particles are "interacting" with the surface of the defined simulation box – which is not appropriate for studying bulk properties. To account for this periodic boundary conditions are utilized. A 2D representation is shown in Figure 3.4. Small boxes are replicated in all directions, and if a particle leaves the box it is replaced by a particle entering from the other side. More advanced techniques allow the use of boundaries for studying different boundary conditions.

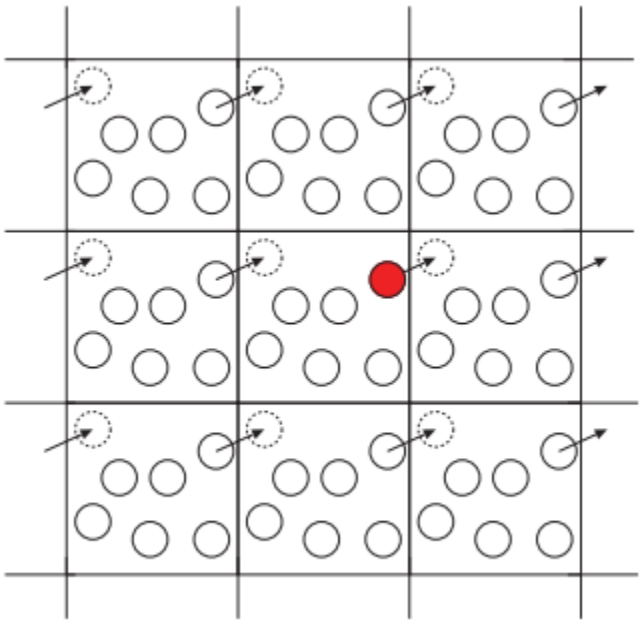

Figure 3.4 – Depiction of periodic boundary conditions used in molecular dynamics simulations[21]

3.2.1 Polarizable Force Fields for Li-ion Electrolytes

Additional difficulty is introduced into accurately modeling molecular force-fields when there are molecules with strong dipoles or ions in solution. In particular, the Li ion is very small and can get very close to either anions or solvents significantly polarizing them. In classical molecular mechanics, this polarization is not accounted for. It has been shown, however, that the polarization of anions and solvents makes up for almost a third of the binding energy between these and Li ions. For this reason, when modeling Li electrolytes, it is important for the models to capture this molecular polarizability.

A number of different methods have been proposed to do this[22] with different trade-offs in efficiency and accuracy of the methods. In this work, the APPLE&P forcefield method developed by Oleg Borodin[23] is used. In the most simplified description, the polarizable forcefield includes an additional term in the model of the Nonbonded potential energy.

$$U^{NonBonded} = U^{ReplusionDispersion} + U^{Coulombic} + U^{Polarization}$$

Detailed information on the models and parameterizations of the variables can be found here[24]

Chapter 4. Combined Economic and Technological Evaluation of Battery Energy Storage for Grid Applications

4.1 Introduction

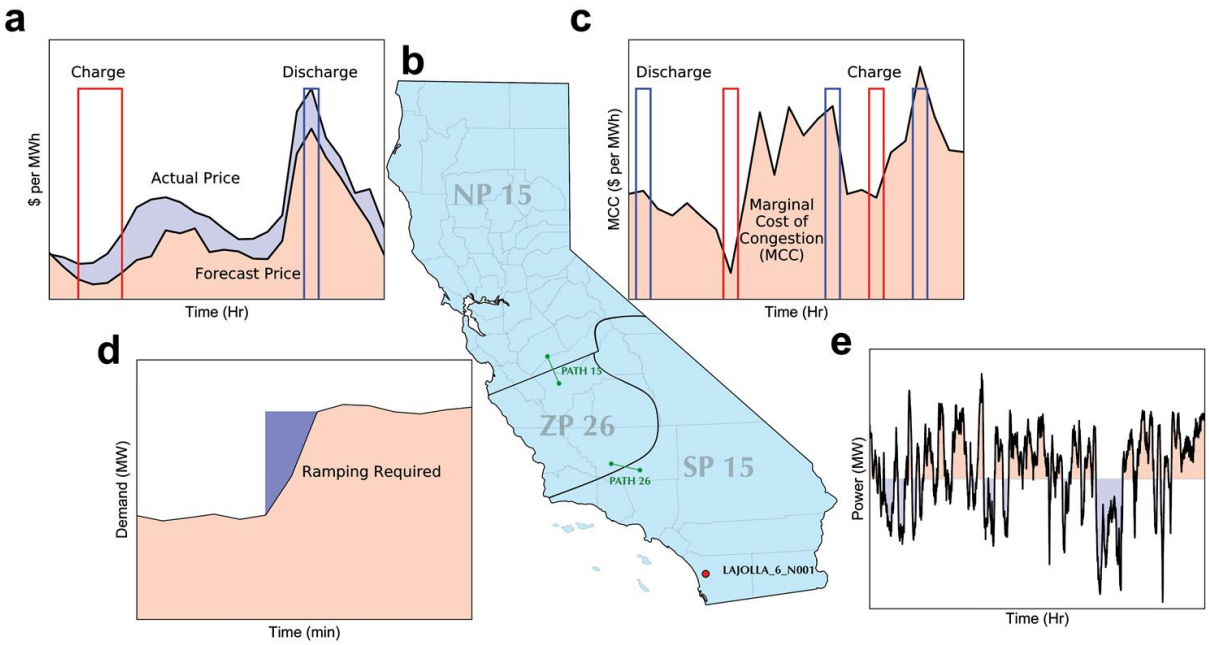

Figure 4.1 California electricity transmission paths and the four applications examined. The central image **b** shows where the data was obtained. The red dot shows the primary node (LAJOLLA_6), from which the pricing and power data used in this paper were obtained for the application duty cycles. The green paths show the location of California's two major transmission paths and the corresponding ancillary service regions NP15 (North of Path 15), SP15 (South of Path 15) and ZP26 (South of Path 15 and North of Path 26). The graphs (clockwise from the top-left) depict the four different application duty cycles considered in this paper. **a,** Energy Time-shift. **c,** Congestion Relief. **d,** Flexible Ramping, and **e,** Frequency Regulation.

Energy storage systems (ESSs) play critical roles in the successful operation of energy grids by better matching energy supply with demand and providing services that help grids function. The use of ESSs require that they are economically viable for the owner of the system. Batteries have drawn much attention for grid-scale storage due to their scalability and ability to

perform a variety of functions. Grid connected batteries provide a wide range of potential revenue depending on the application. For a summary, see Eyer and Corey[25], where they report opportunities for batteries to participate in applications like arbitrage, congestion relief, renewable integration and grid ancillary services. By participating in these applications, batteries help to maintain and improv performance of the grid while potentially providing a source of revenue to the owner. For economically feasible implementation, accurate estimates of revenue are required across battery technologies and applications of the battery to assess the financial potential of the device. From the perspective of modelling revenues, constructing accurate estimates of revenues requires models that take the rules of operation, realistic market prices for services, and the energy and power constraints of the storage device into account.

Previous estimates of revenue vary greatly, based upon the particular market, storage technology, and on the assumptions of the operation of the storage technology[26–29]. For example, a summary by Fitzgerald et. al estimates revenues for load shifting that equate to the operation of a 1MWh battery from near $0 to $274 per day[30]. Such large variations can be attributed to uncertainties in operating conditions. Additionally, the literature often overlooks the interaction of the storage technology with the application itself, assuming similar performance of a technology across different applications. This problem is seen in the evaluation of battery technologies where typical battery testing uses a constant current mode where the electrochemical voltage change is tracked as a function of time.

A more precise understanding of potential revenues and ESS valuation is obtained by making modeling choices as close to real world applications as possible and by testing batteries on schedules that mimic these applications. This includes following the rules of particular markets as closely as possible, choosing schedules for the operation of the storage device using

forecasts rather than known energy prices. Testing batteries using varying dispatches and rates of power dictated by the application will likely lead to values of coulombic efficiency, voltaic efficiency, and total energy efficiency that are different from the values obtained from traditional testing methods like constant current mode.

Sandia National Laboratories separates the revenue-generating grid applications into five categories, with one category devoted to utility customers[25]. By choosing applications that are included in the remaining four categories (electric supply, ancillary services, grid system applications, and renewable integration), we are able to gain a broad understanding of the revenue generation and storage performance across the whole system. The applications we examine within are: time-shift in the day-ahead market (DAM) (Figure 4.1a), congestion relief (Figure 4.1c), flexible ramping (Figure 4.1d), and frequency regulation (Figure 4.1e). The energy shifting timescales of all these applications are relatively short, with the longest discharge or charge for all applications spanning 3 hours maximum. Using data from the California market we evaluate five different battery chemistries. Our calculations use market prices where available from the California Independent System Operator (CAISO) market and are computed over a period of two years of virtual operation of the device. Each revenue calculation produces a duty cycle (power profile, see the definition from Sandia National Laboratories[31]) for the batteries which is used to test the performance of the batteries.

We evaluate revenues with a model of the storage device and show that both revenue and the best application of any ESS are highly dependent on cell level battery efficiency of the ESS. We establish a technique to measure the efficiency of the batteries performing these application-based duty cycles and show that battery efficiency in turn depends on how the battery is utilized to generate the revenues. Because the revenue of each application is dependent on the efficiency

of the battery this results in non-obvious optimal battery/application pairings for revenue generation. This study integrates both the economic evaluation of storage with parameters generated from testing the batteries under the scenario used to construct the revenues and demonstrates the importance of application-based battery evaluation for grid-scale revenue prediction.

4.2 Materials and Methods

4.2.1 Revenue and duty cycle development

The California Independent System Operator (CAISO) provides public market results data via the Open Access Same-Time Information System (OASIS) web-portal[25]. The primary node of interest is LAJOLLA_6_N001 at which energy imports/exports between UCSD and CAISO are settled. LAJOLLA_6_N001 is located south of transmission paths 15 and 26, hence mapping it into ancillary service regions AS_CAISO, AS_SP15 and AS_SP26 and their expanded forms. The 4 application duty cycles were developed to maximize revenue in 4 products that the CAISO offers: Energy time-shift, congestion relief, frequency regulation, and flexible ramping. All of the decisions by the algorithm are made in 'real time' using only data that would be available to an operator in the construction of forecasts on which decisions are based. To start in January 2013 and use past data we required data before January 2013 to construct the forecasts. This is why we obtained 3 years of data, where available, from January 2012.

4.2.2 Time-shift and Congestion Revenues

For the time-shift application we used the DAM data and obtained hourly price and load data from January 2012 to December 2014. As with all price data (DAM and RTM), the price data is made up of three components. The Locational Marginal Price in $/MWh consists of Marginal Cost of Energy, Marginal Cost of Congestion (MCC), and Marginal Cost of Loss components. We downloaded hourly Locational Marginal Prices and their energy, congestion and loss components in $/MWh. We made forecasts of the price and load from January 2013 to December 2014.

The forecasting model considered past prices and load data. Forecasts for each day are made and locked in at 10am the prior day per the CAISO rules. Using these forecasted prices and loads and the physical limits and characteristics of the battery (Figure 4.2), a linear optimization program constructed the schedules for each day. These schedules were applied to the actual load and pricing data to give accurate revenue results. The algorithm also produced a 2-yearlong duty cycle for the application. From the 2-yearlong duty cycle, a representative week-long duty cycle was created. For the congestion application, the methods were almost identical for that of the time-shift application, however, this application is optimized to minimize the expected congestion component. This means that the battery charges when the MCC is low, and discharges when the MCC is high.

4.2.3 Ramping revenue

At the time of the study there was no market currently in place for the ramping application. To model the demand and energy prices we constructed a model based on the description by the CAISO[14]. The flexible ramping requirement is made up of two components, the part due to the net demand forecast change and the component due to uncertainty over this

net demand forecast. The CAISO attempts to find a percentile of the forecast distribution of energy supplied, constructed as a mean plus forecast error variation around the mean. These numbers are constructed by using the running of the market clearing algorithm at the time energy is committed (which has a forecast of demand change) and the value determined right before delivery. For our models, we use an approximation to determine, for any 15-minute interval, whether or not the ramping up or ramping down markets will be operational. The reason we do not need the overall quantity of demand in these markets is that the storage devices we consider are very small relative to the overall markets, and hence we assume that the quantity demanded will be far in excess of the capacity of the storage device.

To do this in the absence of the results from the real-time algorithm that clears the market prices, we approximated the process using 5-minute load data available from the CAISO. This data is for all of California. We used this data to construct forecasts of the 5-minute load using rolling forecasts. These forecasts are then used with the load data to construct whether or not demand for flexible ramping up or down is likely for any 5-minute interval. However, bidding in the RTM is done on a 15-minute basis. We aggregated to 15-minute periods by assuming that if the market is operational for any 5-minute period in the fifteen minutes then it is operational. For our revenue calculations, this means that if we have an energy bid in the RTM for a particular 15-minute period and we have the capacity to offer ramping (typically this means that if we are buying energy at full power we allow the CAISO to reduce power hence allowing ramping down and then obtain less power than we contracted for, the opposite for when we have a bid that is selling energy to the grid) then we can offer it so long as the market is operational. If not, we cannot make a bid in this market. We used a fixed capacity price of $5/MW.

In the CAISO rules, there is no guarantee of actual uptake of energy once a bid is

confirmed. This means that the battery owner loses control of the SoC and must recharge it in the RTM. Due to the CAISO rules, this requires waiting 75 minutes after each use of the battery in the regulation market. The linear optimization program takes this stipulation and the forecasted prices of the RTM into consideration when producing the optimal schedule for operating in the regulation market.

4.2.4 Frequency regulation revenue

For the frequency regulation application, the capacity payment and mileage payment data were available from January 2012 to December 2014. Demand and pricing forecasts were constructed in a similar method to that of the time-shift and congestion cycles. The demand data for the frequency regulation application was simulated. The CAISO only provides a single week of state level demand data in the form of an (Automatic Generation Control) AGC signal. The AGC signal provides the system wide capacity procured every 4 seconds, giving 151200 intervals. The data includes values for the Regulation Down Capacity, Regulation Up Capacity and the AGC signal for procurement. The first two of these are positive, the AGC signal follows the CAISO convention of being positive for energy supplied by generation (Regulation Up) and negative for energy removed by generation (Regulation Down). We aggregated this data to the payment period and constructed probabilities of up or down regulation demand based on the aggregate data (this is relevant since payments are also on the aggregate).

There are instances for which the AGC signal capacity is higher than the system wide capacity indicated. For these we set the AGC signal equal to capacity (this is AGC Trimmed in the data). For any four second interval (observation) we compute the proportional take-up of capacity in any period whilst preserving the sign indicating regulation up or down. As discussed

in the previous subsection on ramping, application of the battery in this market (non-REM regulation) results in no guarantee of uptake of the offer for regulation services. We follow a similar strategy as in the last paragraph on ramping to ensure the battery does not exceed its SoC limits. Downtime waiting for charge/discharge in the RTM reduces the value of the battery in this application.

To model week to week variation through the two years we followed an approach in Donadee and Wang that models demand using an AGC signal at the hourly level relevant for cost calculations.[26] In this model demand for up and down regulation is modelled as a function of the previous hour demand and a function of the AGC signal plus four variables that capture intraday seasonality using a Fourier approximation. We ran the regression for the week of data from CAISO to estimate the coefficients of the model separately for regulation up and regulation down and estimated the residuals from these regressions. The two year-long demand sequence is then generated from these regressions (again separately for regulation up and down) using a nonparametric bootstrap.

4.2.5 Cell level testing

Tests were carried out on the batteries using an Arbin Laboratory Battery Testing cycler. Each duty cycle was carried out on a separate battery. The Lithium-Ion (LFP, NMC) and Nickle Cadmium (NiCd) batteries were purchased from *Tenergy*[32–34]. The Lead-Acid (PbA) battery was purchased from *EnerSys*[35]. The Sodium-Ion (Alv) battery was provided by *Alveo Energy*[36] and was under development at the time. Due to the availability of the batteries from *Tenergy*, the LFP and NiCd batteries were tested using two different form factors. These batteries differed only in the capacity of the battery. Using the Ragone method to calculate the correct *max* S^E and *max* P^C

for each application ensured that the different sizes of the batteries had no impact on the efficiency calculations.

4.2.6 Ragone

Prior to each Ragone test, each battery underwent 3 break-in cycles, cycling at constant power at rates equivalent to E/P=2 according to the manufacturers advertised cell capacity between the manufacturer's specified voltage limits. A power cycle at a rate equivalent to E/P=20 was then performed before carrying out the Ragone test. The Ragone test was executed by power cycling the battery at rates equivalent to E/P ratios of 20, 10, 5, 2, 1. The Ragone data shown in Figure 3c, d is averaged over the results of 10 of each battery chemistry.

As described in Fig. 3, the estimations of $max\ S^E$ and $max\ P^C$ were made from the Ragone plot for each battery and each application for E/P ratios of 1 and 3. Subsequently, $max\ \gamma_B$ was interpolated from the voltaic efficiency vs power plot. Originally, we had used the energy efficiency at each power (Fig. 3b), however, this often resulted in an under-estimation of the efficiency, and so we switched to using the voltaic efficiency. For the time-shift, congestion, and frequency regulation applications, the SoC limit (20-80%) was selected to ensure that all battery chemistries could safely, and repeatedly complete the week-long duty cycles. This limit was primarily based on the performance of the PbA and NiCd batteries, whose voltaic efficiencies were difficult to estimate. Due to the overestimation of the efficiency, the battery rapidly approaches, and surpasses its voltage limits, causing failure. While extending the state of charge limits allows a larger portion of the battery to be used, it ultimately leaves less room for error.

4.2.7 Time-shift and congestion testing

Prior to each duty cycle, the batteries were power cycled at the selected operational power for each duty cycle (*max* P^C , and *max* P^D). The maximum charge capacity of this cycle was used to calculate the SoC for the rest of the duty cycle. The batteries were discharged at power *max* P^D to their advertised lower voltage limit, and then recharged at power *max* P^C to the correct SoC to begin each day. For the time-shift and congestion applications, the economic results set this to 20% of the entire SoC range. In current literature batteries are often charged and discharged to SoC limits based on capacity[7]. This artificially sets the coulombic efficiency to 100%. By adding this top-off step we are able to separate the energetic efficiency into its coulombic and voltaic components. This separation helps us to better understand the effects of the duty cycles on the chemistries

4.2.8 Ramping testing

As there was no available data provided by the CAISO on the shape of the ramping cycle, a linear ramp from 0 *Watts* to *max* P^C, or *max* P^D,was used for each event of the duty cycle. $P^C/2$. This operational power was used for the initial cycle and the topoff steps during the ramping cycle. This had the effect of altering the operational SoC range of the ramping duty cycles to between 40-60% of maximum capacity. The top off step days brought the SoC to 50% at the start of each day. This beginning SoC was dictated by the shape of the application duty cycles where there is a possibility that either ramping up or down could generate the most revenue. We chose to test the ramping duty cycles in this manner to respect the power limits imposed by the battery and the E/P ratio.

4.2.9 Frequency Regulation testing

The CAISO only provides a week-long snap-shot of the power profile of the frequency regulation signal. This is in the form of an AGC signal with fluctuations in power every 4 seconds - giving 15200 intervals, and the regulation up and down capacity demand profiles which fluctuate every 15 minutes. To simulate the action of an ESS performing this application, we used the information provided by the economic simulation on when it would be most profitable for an ESS to participate. This information was provided in the form of a duty cycle which fluctuates on a 15 minutes basis where the ESS is either participating, resting, or charge balancing (returning to 50% of its SoC). As an example, a 2 hour snap shot of the duty cycle for an E/P = 1 ESS is shown as $[A_1,A_2,0,0,0,0,B_1,B_2]$. Where A denotes that the ESS is participating in the frequency regulation application, 0 denotes that the ESS is resting, and B denotes the ESS is charge balancing. The subscripts indicate application/charge-balancing pairs. The CAISO rules dictate that the ESS owner must wait 75mins before charging/discharging in the RTM after a successful bid. As the energy uptake of participating in the application is unknown prior to the completion of the application, and the ESS is limited by maximum power bounds, if an ESS participates in the application for 15 minutes, a 15-minute period must be allotted to ensure with certainty that the SoC of the ESS is restored. By the above CAISO rule, this charge balancing period must be at least 75 mins after the application period. If E/P = 1, the maximum number of consecutive periods that the battery can participate in the frequency regulation application is 2. The battery begins each period at 50% SoC. There is potential for the application to demand full power for the whole period, which would use 25% of the available energy. Therefore, to ensure certainty of operation, an ESS with an E/P ratio of 1 can only participate in 2 consecutive periods of the application when its full power capacity is bid. Similarly, if E/P = 3, the maximum number of consecutive periods that the battery can participate in the frequency regulation application is 6.

This has the interesting effect where the battery never has to undergo a rest state as the battery can participate in the frequency regulation application during the 75-minute waiting period required before charge-balancing. A 3 hour snap shot of the duty cycle for an E/P = 3 ESS is shown as [A_1,A_2, A_3,A_4,A_5,A_6,B_1,B_2, B_3,B_4,B_5,B_6].

After the duty cycles were finalized, each battery chemistry was tested at least 2 times for each application at E/P ratios of 1 and 3. The efficiency data showed good reproducibility both in the values of the efficiencies, and in the inter-day efficiency trends that arise from the different power profiles on each day. The efficiency data presented in the paper is averaged from the number of batteries tested on each application at each E/P ratio.

4.3 Battery Model

Grid connected batteries in the form of ESSs are often complicated and contain power electronics and maintenance systems. The interaction of these systems with different battery chemistries themselves is complicated. For example, the performance of Li-ion batteries is often more temperature dependent than that of Lead-Acid batteries[8], and so the chemistries may require different thermal management systems. This complication is further enhanced by the interaction of the power electronics with application duty cycles. Inverters, for example, are designed for a certain power output and operate less efficiently at other powers[9]. Therefore, an inverter would likely perform at a lower efficiency during the frequency regulation application (which has many power fluctuations) than the time-shift application. Rather than guessing at the efficiencies of the power electronics and maintenance systems, we excluded their effects from this paper. The present study focuses on the performances of the fundamental building blocks (cell-level batteries) of these storage systems for a variety of applications while future work will

take the effects of additional variables such as power electronics into account.

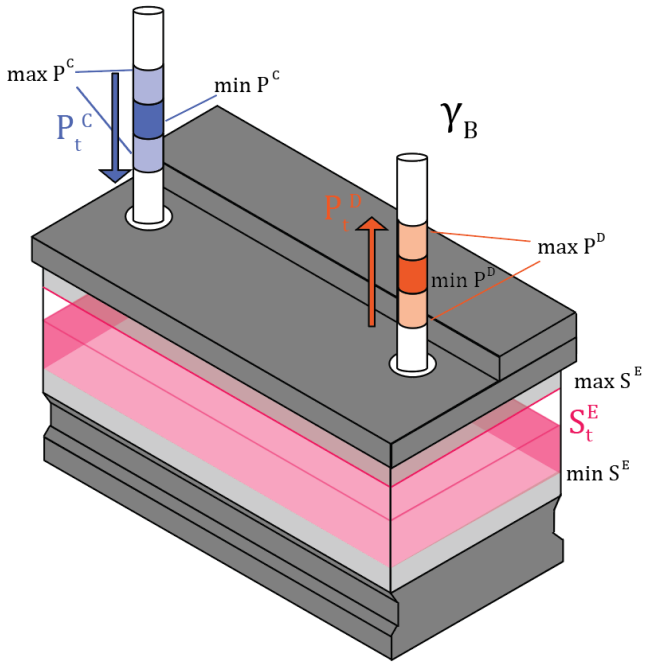

Figure 4.2. The model of a battery used in the economic modeling of the duty cycles. The algorithms developed considered the following parameters: Charge rate (*max* , *min* , where is the average power taken from the grid (charge power) during time step *t, max* and *min* are the maximum and minimum amounts of power that can be taken from the grid by the battery respectively*;* Discharge rate (*max* , *min* , *)* where is the average power received by the grid (discharge power) during time step *t, max* and *min* are the maximum and minimum amounts of power that can be delivered to the grid by the battery respectively; Power Electronics efficiency *()*Self-Discharge Efficiency *()*; Battery efficiency *()*; and Available energy (*max* , *min* , *)* where is internal energy of the battery at time *t, max* and *min* are the maximum and minimum amounts of energy that the battery can store in its operational charge window respectively

The storage device is modelled by a discretized equation governing the state of energy (Figure 4.2). The state of energy S_t^E at time *t* follows the process

$$S_t^E = S_{t-1}^E \cdot \gamma_{SD} + \gamma_{PE} \cdot P_t^C t - \gamma_B^{-1} \cdot P_t^D \cdot t$$

where S_{t-1}^E is the state of energy at the end of the previous time step, $max\, S^E$ is measured in MWh. The time step *t* is either 15min (in the real-time market, RTM) or 1hr (in the DAM) depending on the application. P_t^C and P_t^D are the average charge and discharge rates (the rate of power that the grid either gives to, or receives from, the ESS) respectively during timestep *t,* measured in MW. It is important to note here that the power throughout a single timestep could vary considerably, as it does in the frequency regulation application. To relate these values to S_t^E the power must be converted to an energy (measured in MWh) by multiplying by the time step *t.*

The parameters γ_{SD}, γ_{PE}, and γ_B are the self-discharge, power electronics, and battery energy efficiencies respectively. Because our tested systems have no power electronics and low self-discharge rates, it is reasonable for us to assume that both γ_{SD} and γ_{PE} are equal to 1. Here $\gamma_B \leq 1$, indicating that to supply the grid at an average rate equal to P_t^D, the battery must discharge at an average rate of $\gamma_B^{-1} P_t^D$, which is always greater than, or equal to P_t^D. For all applications, physical constraints on the battery are imposed, so the internal state of charge (SoC) remains within a preset range (20 – 80% SoC). Note that CAISO penalizes the resource if energy is promised and not delivered. The 20-80% SoC range is the largest range we could use while ensuring that all of the batteries safely completed the entire duty cycles. The amount of charge and discharge in any time period is constrained by the maximum power rating which determines the maximum and minimum charge and discharge rates ($max\, P^C$, $min\, P^C$, $max\, P^D$, $min\, P^D$). The economic model was made for a 1MWh ESS (the power rating can vary) and scales linearly for

any sized ESS.

The energy to power (E/P) ratio describes the ratio of the available energy of the ESS to the maximum charging power[37]. The higher the E/P ratio, the more complicated or richer the duty cycle. This is because when a profitable cycle is expected, the optimal use of the ESS involves utilizing the maximum amount of discharge or charge possible, bounded by both the power rating and the state of energy. For a higher E/P ratio, the set of possible charge/discharge cycles for each application rises. The optimization procedures thus are now choosing from a larger set, hence most often we obtain more charges/discharges and therefore a more complex set of duty cycles. In this paper, we develop duty cycles for ESSs with effective E/P ratios of 1 and 3. We then present the results of the performances of several battery chemistries performing these duty cycles. Batteries have a limited amount of energy, and so for our cell level testing, adjustments to the E/P ratios were realized in adjustments in the power used by the battery. The parameters discussed above are intrinsic to the ESS that are common across all applications. The application specific optimizations are explained briefly below and in more detail in the methods section.

4.4 Revenue and Duty Cycles

The application duty cycles were primarily designed to maximize the potential revenue of an ESS in one of the products that the CAISO offers. Our approach followed and extended the Electric Power Research Institute (EPRI) methods and tools for evaluation of electricity storage laid out in the 2013 handbook written by Sandia National Laboratories [38] as well as being tailored towards the California market. The handbook outlines potential grid applications and energy storage technologies that could take advantage of these. The methods involve identifying

opportunities, understanding the requirements of the grid, distinguishing between monetizable and incidental benefits, and finally creating energy storage business cases. Prices used were those for the LA JOLLA 006 node, which is the appropriate node for a study out of the University of California, San Diego. For each application, we chose a representative set of cycles that occur often.

The time-shift application in the DAM works by charging the ESS when the forecasted price of energy is low, and then discharging the ESS when the forecasted price of energy is high[26,27,29,30,39,40]. The congestion relief application is similar to that of energy time-shift. However, the batteries performing this function serve to free up bottlenecks in electricity transmission and so more charge/discharge events occur[31]. The flexible ramping application accounts for power fluctuations required to adjust to energy delivery over periods of the order of 5 minutes[30]. Lastly, the frequency regulation application is designed to synchronize the supply and demand on electricity grid[26,40,41]. It is important for the storage system performing this task to be able to respond quickly to pulsed-power, regulation up, and regulation down signals. It is important to note that the regulation application assumes that the ESS is operated in the non-REM (Regulation Energy Management for a Non-Generating Resource) mode. This means that the owner of the ESS maintains control over the state of charge (SoC) of the device.

For calculating revenues and duty cycles for the time-shift application in the DAM, we obtained price in the form of the Locational Marginal Price, load, and forecast load data from the CAISO website for hourly prices over the period from January 2012 until the end of 2014. We used this data to generate forecasts for each hour of each day for the last year of this period using a model for each hour of the day incorporating past prices (1 year) and load data. Forecasts were made at 10 a.m. the day prior to scheduling the storage device (this is the rule for participating in

the California DAM) using only past data. The forecast data was used in conjunction with a linear programming optimization to construct a schedule for each day that maximized expected revenues based on the forecasted prices, where use of the storage device was constrained by the efficiency and energy of the device as per the described model (Figure 4.2) for the battery. This optimization produced actual daily revenues based on the actual prices realized, as well as a duty cycle for the operation of the battery. The Locational Marginal Price consists of Marginal Cost of Energy, Marginal Cost of Congestion and Marginal Cost of Loss components. For the congestion relief application, we undertook the same steps as for the time-shift application, but schedules are optimized to minimize the congestion at the node as defined by the marginal cost of congestion. This has the effect of charging when congestion is low and discharging when congestion is high.

For the regulation and ramping markets, revenue is gained through offering the service (in the form of capacity payments), as well as energy payments when called upon to provide the service. By the CAISO rules, capacity payments are payments made for providing the opportunity for CAISO to add or remove energy, which are paid for regardless of whether or not energy is provided. Our optimization algorithm used simulated data and capacity payment data. Forecasts were made 75 minutes prior to scheduling the storage device (this is the rule for participating in the California RTM) using only past data. For regulation markets, a single week of state level demand data was available at the time of the study. Capacity payment data was available for the regulation market, we constructed forecasts for prices as in the time-shift application. For the ramping market, at the time of the study, no market was in place, so we built a model based on the description by CAISO and used a fixed capacity price of $5 per MW. This is the lower end number that the CAISO used in their explanations for how it might work in their Draft Technical Appendix published in June 2015[42]. In these two applications, the ESS owner

cannot determine the SoC because it is unknown if the service will be called upon. We ensure that the SoC stays within its limits by tracking bounds on the SoC (which are known) and charging/discharging in the RTM to return the battery to a known SoC periodically.

For the time-shift and congestion applications the duty cycles produced fluctuate hourly for two years, for the regulation and ramping applications they fluctuate every 15 minutes for two years. These duty cycles were condensed into schedules for battery testing by choosing a one-week duty cycle representative of the two years of cycling.

4.5 Important Battery Parameters and Their Relationships

There is a large amount of research on the advantages and drawbacks of a variety of potential electrochemical storage technologies for their use on the grid[37,38,41,43–45]. Five different battery chemistries were used for testing in this paper. Li-ion batteries containing (lithium iron phosphate — LFP) and $LiNi_{1/3}Mn_{1/3}Co_{1/3}O_2$ (nickel manganese cobalt oxide — NMC) cathodes paired with a graphite anode, as well as nickel cadmium (NiCd) and lead-acid (PbA) batteries were purchased from reputable vendors (described in the Methods section). Finally, Alv refers to an aqueous-based sodium-ion () battery under development by *Alveo Energy*[36].

Battery manufacturers often only supply a single energy rating for a singular rated current. Although this is a common testing method that is arguably sufficient for common battery applications, to maximize the revenue obtainable on the grid, the relationship between the power output and energy capability need to be carefully considered. We present a protocol utilizing Ragone plots[46] that allow us to select the optimum charging and discharging power to be used in order maximize the revenue obtainable by the storage device. This method enables us to vary the E/P and SoC ratios utilized, and to partially account for the different energy efficiencies of each

battery chemistry, in order to maximize the battery's utility. By using this method, we more accurately depict how a battery would be used on the grid and can obtain more accurate efficiency and revenue estimates.

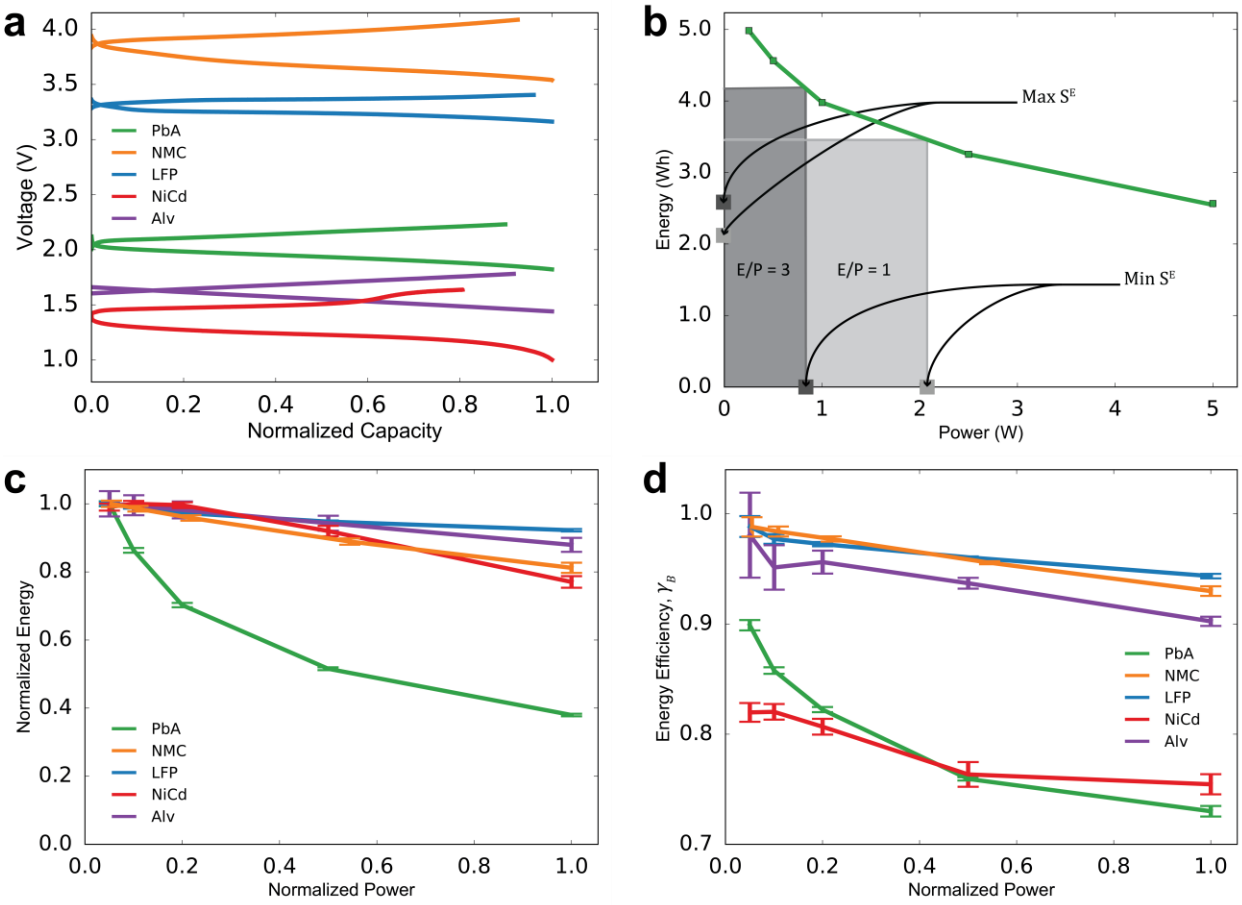

Figure 4.3. Preparatory electrochemical testing and Ragone data. **a,** Charging/discharging the five batteries at constant power for one hour. Charge and discharge power are the same, so current is higher on discharge than charge. **b,** An individual Ragone of a *PbA* battery. The battery was cycled at constant power at rates corresponding to E/P ratios of 20, 10, 5, 2, and 1 according to the rated energy of the battery (from left to right). The green line shows the splined fit of the charge energy of the battery. The chosen power and energy corresponding to operation of E/P=1 are shown in light gray, for E/P=3, they are shown in dark gray. Light gray squares indicate *max* and *max* for E/P=1, dark gray squares indicate the same values for E/P=3. The value of *max* is equal to the SoC range multiplied by the total available energy at *max* . **c,** Normalized Ragone data of the five tested battery chemistries. The batteries were cycled at constant power at rates corresponding to E/P ratios of 20, 10, 5, 2, and 1 (from left to right). Curves drawn show the splined fit of the charge energies of the batteries. Error bars show the standard error of the charge energy at each rate with a sample size of 10 batteries of each chemistry. **d,** Energy efficiency of the five chemistries at rates corresponding to the E/P ratios mentioned in figure c. Curves drawn show the splined fit. The error bars show the standard error of the energy efficiency at each rate with a sample size of 10 batteries of each chemistry.

Predicting the efficiency and available energy at an operational power is difficult. To ensure the safe operation and successful completion of each duty cycle by each of the chemistries, the cells were cycled in a limited SoC window, which, as previously mentioned, we chose as 20-80% of the maximum capacity of each battery charged at $max\ P^C$. This window was based primarily on the performance of the PbA and NiCd batteries, whose efficiencies were more difficult to predict. The larger cell to cell efficiency variation of the PbA and NiCd batteries when compared to the Li-Ion batteries is seen in the larger standard error bars shown in Figure 4.3d. This means that in the economic model described above $max\ S^E$actually refers to the energy of the battery corresponding to the middle 60% of its entire energy capacity range at a given power, $max\ P^C$. As there are penalties imposed for being unable to deliver promised energy on the grid, ESSs on the grid operate in a similar manner.

Applications on the CAISO grid involve dispatches of controlled amounts of power for predetermined periods of time[47]. The effect of charging and discharging at the same constant power for 1-hour-long periods is shown in Figure 4.3a for each chemistry. Because the voltage is lower during charge than discharge and

$$P = I \cdot V$$

where P is power, I is current, and V is voltage, for equal power the current during discharge is higher than during charge. This means the battery will run out of capacity if subjected to many of these steps. To maximize the revenue of the battery while operating in a safe SoC range we set

$$max\ P^D = \gamma_B \cdot max\ P^C$$

To select the optimal value of $max\ P^C$ to be used by the battery in each application, we utilized our Ragone diagrams of each chemistry. These diagrams also allowed us to estimate the value of γ_B for each chemistry in each application. An individual Ragone diagram of a PbA

battery is shown in Figure 4.3b. The battery was cycled at rates corresponding to E/P ratios of 20, 10, 5, 2 and 1 (from left to right) according to the rated energy of the battery. To obtain the correct $max\ P^C$ and $max\ S^E$ to use for the applications, the SoC range needed to be considered. We used the gradient of the splined Ragone diagram to solve the following equation to find the optimum energy and power values.

$$max\ P^C = \frac{(SoC_{Lim}^{Max} - SoC_{Lim}^{Min}) \cdot Energy}{E/P\ Ratio}$$

Here, *Energy* refers total available energy of the battery should the entire SoC be used, SoC_{Lim}^{Max} is the upper state of charge limit (as a proportion of available *Energy)* which was set to 0.8 in for this paper, SoC_{Lim}^{Min} corresponds to the lower state of charge limit and was set to 0.2. The operational energy, $max\ S^E$, and maximum power, $max\ P^C$, used for E/P = 1 are shown by the light gray rectangle, for E/P =3 they are shown by the dark gray rectangle. $Max\ S^E$ is given by

$$max\ S^E = Energy \cdot (SoC_{Lim}^{Max} - SoC_{Lim}^{Max})$$

$Max\ S^E$ and $max\ P^C$ are shown by the small light gray and dark gray squares for E/P = 1 and E/P = 3 respectively. Once these values are found, γ_B is estimated by interpolating the voltaic efficiency of the battery at $max\ P^C$.

Figure 4.3c and Figure 4.3d show how the available energy and efficiency of each of the chemistries vary with power. The batteries were cycled at rates corresponding to E/P ratios of 20, 10, 5, 2 and 1 (from left to right) according to the rated energy of the battery. As well as providing us with a method to accurately replicate how a battery would be used on the grid, these Ragone diagrams give us an indication of characteristics of the chemistries that might be important for different applications. For example, although NiCd had generally poor efficiency

(Figure 4.3d**)**, it maintained good rate performance (Figure 4.3c**)** when compared with PbA.

4.6 Relationships Between Duty Cycles and Battery Chemistries

Once the parameters for each application and chemistry were calculated, the batteries were tested on the duty cycles. The time-shift and congestion applications involve periods of deep charge/discharge[26,27,37,48] whereas the ramping and frequency regulation cycles are power based applications and move smaller amounts of energy with each charge and discharge[26,49,50]. The duty cycles include an additional "top-off" step which allows us to extract from the efficiency its coulombic and voltaic components. The efficiency of each battery is calculated for each day of each duty cycle. Interesting inter-day variations occur due to the nature of the studied applications. In Figure 4.4, we show the average weeklong efficiencies of each of the battery chemistries undergoing the different applications at E/P = 1.

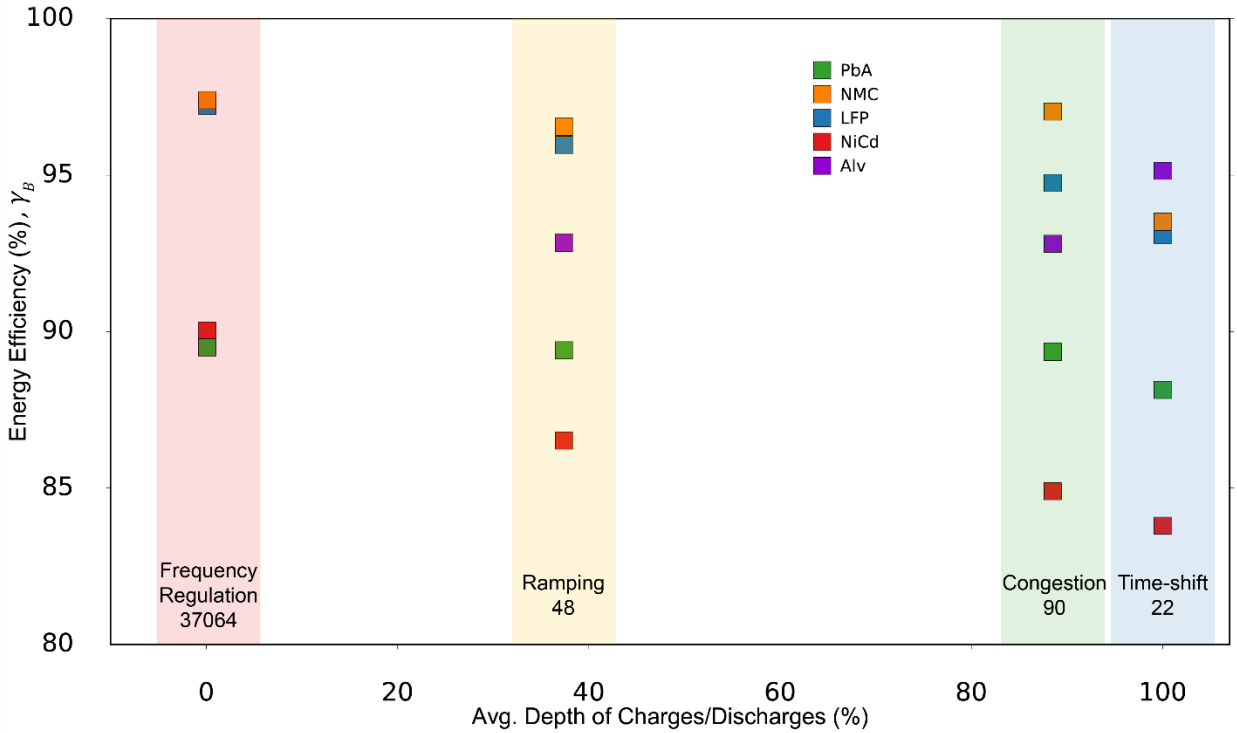

Figure 4.4 Energy efficiencies of batteries performing the application-based duty cycles. E/P = 1 duty cycles are characterized by the average depth of charges/discharges and by the number of charge/discharge events per week. Results for: *Frequency Regulation* (Red box); *Ramping* (Yellow box); *Congestion* (Green box); and *Time-shift* (Blue box) are shown. The numbers below the labels show the number of charge/discharge events per week. The average energy efficiency from the week-long duty cycles are shown for each battery chemistry. At the time of testing the *Alveo* battery, the frequency regulation duty cycle had not been finalized and so the efficiency result is not included.

It is known that the efficiency of a battery varies greatly with its chemistry[37,43,47,51,52]. For all the duty cycles, the Li-ion chemistries (NMC, LFP) had the highest efficiencies of the commercial batteries tested, whereas the NiCd chemistry had the lowest efficiency. The efficiency of the sodium-ion batteries (Alv) were impressive, yet inconsistent. These batteries were under development at the time which likely led to large inter-battery variance. The results for E/P = 3 follow a similar trend.

Evaluating the performances of the chemistries undergoing the duty cycles yields two key insights. First, the duty cycles have substantially different effects on the efficiencies of the batteries. For all the commercial batteries, the efficiency during the time-shift application was

always the lowest and was always highest for the frequency regulation application. Second, the magnitude of the influence of the duty cycles on the efficiencies varies with each chemistry. In moving from the time-shift to frequency regulation duty cycles, the energy efficiency, γ_B, of the NiCd chemistry changes from 83.8% to 90.3%, a difference of 6.5%. For the PbA chemistry, γ_B changes only from 88.1% to 90.0%, a difference of 1.9%. This mismatch in efficiency between chemistries and duty cycles becomes important in evaluating the use of a particular chemistry in different grid-scale applications, as is shown when combined with the revenue results.

.

4.7 Influence of Battery Efficiency on Revenue

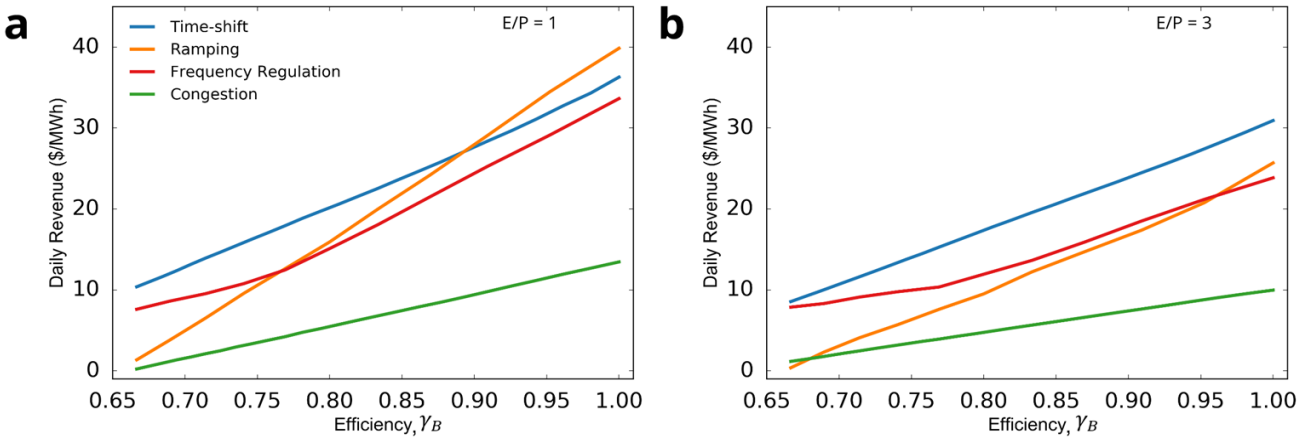

Figure 4.5 The revenue vs. the efficiency for the different application duty cycles. **a,** E/P=1; **b,** E/P=3.

The results in Figure 4.5 show how revenues improve as the energy efficiency, γ_B, improves. For applications that require deep discharge – time-shift and congestion – improvements arise as for each opportunity to generate revenue, a larger amount of energy can be discharged to, or taken from, the grid. The linear increases in revenue follow as increases in

efficiency simply increase the payment for each cycle. For regulation and ramping, the majority of revenue arises from capacity payments. The increasing slopes of the effect of efficiency on revenues arise as the greater available energy allows the storage to offer proportionally greater energy over time.

Table 4.1 Average efficiencies and corresponding revenues for each duty cycle and chemistry combination for batteries undergoing the duty cycles at E/P=1.

Duty Cycle	Revenue	Battery Chemistry					
		100%	PbA	LFP	NiCd	NMC	Alv
Time-shift	Efficiency (%)	100.0	88.1	93.1	83.8	93.5	95.1
	Revenue ($)	36.3	26.2	30.1	22.9	30.5	31.8
Congestion	Efficiency (%)	100.0	89.4	94.8	84.9	97.0	92.8
	Revenue ($)	13.5	9.1	11.4	7.4	12.3	10.6
Ramping	Efficiency (%)	100.0	89.4	96.0	86.5	96.6	92.8
	Revenue ($)	39.9	27.1	35.7	23.8	36.5	31.8
Regulation	Efficiency (%)	100.0	89.9	97.2	90.0	97.4	N/A
	Revenue ($)	33.6	24.3	31.1	24.4	31.2	N/A

To establish a more real-world evaluation of the value of different chemistries in different applications, Table 1 reports the average efficiencies and the revenues at those efficiencies where the efficiencies are found from the batteries performing the appropriate duty cycles at E/P=1. Examining revenues based on experimental efficiencies allows greater insight into the relationships between the chemistry choices and the applications of the batteries. First, revenue calculations at full efficiencies are misleading, not only in the size of the revenue, but also, they indicate that the best application of the battery is for applications like time-shift or ramping. The results show that at 100% efficiency there is statistically significantly higher revenue for time

shift than for regulation. However, for high efficiency chemistries such as those based on Li-ion (LFP, NMC), more revenue is generated in regulation than time-shift because of the differences in efficiencies across applications. The second implication that arises is that there can be a strong variation of efficiencies across applications that shift the relative value of any application to each technology. For all chemistries, efficiency is higher for the duty cycles that require lower fluctuations in the SoC, like regulation. However, the relative gains in efficiency (across duty cycles) differ across chemistries, being small for PbA and larger for the other chemistries. This has the result that for most of the chemistries regulation improves revenue relative to time-shift, which is not true for PbA. Finally, for a low revenue application such as congestion relief, differences in efficiencies are far less important since the revenue is relatively flat over the efficiency of the battery, so lower efficiency chemistries are relatively more valuable in these applications over the high efficiency chemistries.

4.8 Conclusion

There is substantial variation in the potential revenue generation reported in the literature. By making modeling choices that replicate real world applications as closely as possible and, when it is available, by using large amounts of data to construct our models we have provided a reliable understanding of the potential revenues obtainable by an ESS on the California grid. We also developed a technique for accurately measuring the performance of cell-level battery chemistries undergoing duty cycles representative of these applications. This technique demonstrated the importance of understanding the efficiencies and rate performances of batteries subject to use.

More importantly, contrary to current literature we show that to accurately gauge the

potential revenue of an energy storage technology on the grid it is insufficient to assume constant efficiencies across different applications. As an example, for the LFP battery, if one were to assume that the efficiency of the time-shift application (93.1%) was consistent across all of the battery applications, this would result in a substantial error in the calculations of revenue. For the congestion, ramping and frequency regulation applications, the percentage error in calculated revenue would be 6%, 11%, and 15% respectively. The combined results of our economic modeling and cell level testing demonstrate that different grid-scale applications affect the energy efficiencies of different battery chemistries in different ways. These effects alter the relative value of each battery chemistry in each application, potentially resulting in a change in the optimal chemistry-application parings. To gain further insight into the different effects that application duty cycles have on ESSs, a larger variety of battery chemistries and energy storage technologies (including larger scale and more complete storage systems) will be tested. Longer term testing will be completed to observe the effects of different application duty cycles on the lifetime performance of the different energy storage technologies. Finally, additional duty cycles will be created by exploring other applications as well as stacking multiple applications together.

Combining the effects of efficiency, lifetime performance, and cost analyses of storage technologies with respect to each grid-scale application will provide a more nuanced understanding of the relative benefits of different technologies to be used to for grid-scale storage. This study illustrates the importance of considering the relationships between applications, chemistries, and efficiencies, to obtain potential revenues of ESS on the grid and could result in a paradigm shift in the way that energy storage technologies are evaluated for grid-scale use.

Chapter 4, in full, is a reprint of the material “Combined Economic and Technological Evaluation of Battery Energy Storage for Grid Applications” as it appears in Nature Energy, D. M. Davies, M. G. Verde, O. Mnyshenko, Y. R. Chen, R. Rajeev, Y. S. Meng & G. Elliott. The dissertation author was the primary investigator and first author of this paper.

Chapter 5. Electrochemical Cell Cap for Liquefied Gas Electrolyte

5.1 Background

Electrochemical storage devices have been in use for years. The electrochemical energy storage device itself is typically made up of one positive electrode and one negative electrode separated by electrically insulating material such as in a battery or an electrochemical capacitor. Conventional electrochemical storage devices use electrolytes which are a liquid under standard conditions. Typically, these electrolytes are injected into a cell in a liquid state and at atmospheric pressure. This injection may occur with no cap on the device, after which a cap is placed onto the device and sealed shut. Alternatively, electrolyte injection may occur with a cap on the device with a smaller electrolyte injection hole in the cap, after which a rubber or metal stop is placed into the hole which creates a seal. Typically, the electrolyte injection and the material insertion to plug the hole are done in two steps. This disclosure focuses on electrochemical devices which utilize electrolyte materials and solvents that are gaseous at standard room temperature of +20 ℃ and standard pressure (approximately 1.01325 bar). Because of the gaseous nature of these electrolytes, conventional liquid electrolyte injection may not be feasible.

5.2 Summary of the Invention

Embodiments of the present disclosure relate to cap devices which seal the device, systems, and components thereof, in particular, of an electrochemical energy storage device that uses a liquefied gas solvent, for example, in the electrolyte thereof. Other embodiments of the present disclosure relate to methods of preparing and methods of using the cap devices, systems, and related components thereof. One embodiment is an electrochemical energy storage device cap, which enables injection of a liquefied gas solvent or electrolyte. These solvents and

electrolytes may include highly volatile solvents which are typically gaseous under standard conditions of standard room temperature of +20 °C. and standard pressure (approximately 1.01325 bar). The solvent may be transferred to the cell in either gaseous or liquid form while the electrolyte, composed of liquefied gas solvent and other liquids and solid including salts, can be transferred in a liquid form. If mass transfer is in liquid form, the pressure within the mass transfer tube must be greater than the vapor pressure of the material at the temperature of the mass transfer portion. If mass transfer is in gaseous form, the pressure within the mass transfer tube should be less than the vapor pressure of the material at the temperature of the mass transfer portion. In some embodiments, the injection process occurs under a differential pressure between the pressure within the mass transfer tube and the internal pressure of the cell. The pressure differential between mass transfer tube and cell may be used to open a plug or a valve on the cell cap when pressure within the mass transfer tube is higher than the pressure internal to the cell housing. When the pressure differential falls to near zero, this valve will seal and prevent mass escape even if the external pressure is lower than internal pressure within the can. The seal will not open even under excess pressure within the device. This type of one way pressure activated plug or valve is commonly known as a check valve. It should be noted by those skilled in the art that check valves, or components acting as such, have been installed on electrochemical devices, such as batteries and electrochemical capacitors, previously. However, in these typical uses, the check valve is used to purposely release excess pressure buildup within the device as the device ages or cycles or experiences over charge abuse. This pressure release allows the device to continue to operate normally or fail safely without burst. In the present invention using the liquefied gas electrolytes, a high internal pressure is normal to the operation of the cell and it is not desired to release high pressure through the check valve. The check valve is used only to fill

the device with the liquefied gas electrolyte, after which it is sealed shut permanently during use. Another benefit to the check valve is the release and recycling of the liquefied gas electrolyte after device use. One may mechanically force open the check valve which will allow the liquefied gas electrolyte to evaporate through the check valve. The evaporated gas may be captured for reuse. Further, the now evacuated cell may potentially be refilled with liquefied gas electrolyte again to continue operation. This may extend the useful life of the device. Embodiments also feature a check valve which uses a biased member or spring to require a minimum differential pressure to open.

Other embodiments feature a spring-less check valve which uses no spring to force a seal to form but instead relies entirely on a non-zero pressure differential to push a plug to seal the valve. Other further embodiments include a method in which vacuum is first pulled on the internal housing and cell components prior to liquefied gas solvent or liquefied gas electrolyte. The present disclosure also provides a check valve having a metallic housing. This metallic housing may be electrically connected to either the positive or negative electrode of the device such that the check valve itself may also serve as an electrical current pathway to the external load. An electrochemical device is disclosed herein. In some embodiments, the electrochemical device may comprise a cell housing, two or more electrodes, an electrolyte comprising a liquefied gas electrolyte solvent, and a cap with a check valve. The check valve can be configured to seal shut under higher internal cell pressure compared to outside cell pressure. In some embodiments, the electrochemical device may comprise an independent cap housing. In some such embodiments, the check valve can be built into the cap housing. In some embodiments, the check valve may act as an electrical contact to one of the two or more electrodes. In some embodiments, the check valve may comprise a spring configured to create a

minimum differential pressure A method of preparing an electrochemical device is also disclosed herein. The electrochemical device can be any one described below in the Detailed Description or described elsewhere herein. The method may comprise transferring the liquefied gas solvent into the cell housing by connecting the liquefied gas solvent to the check valve. The method may further comprise building a pressure differential between the interior and exterior of the cell housing. In some embodiments, the pressure differential may be created by a temperature differential. In some embodiments, the pressure differential may be created in gaseous argon, gaseous nitrogen, gaseous oxygen, gaseous carbon dioxide, gaseous hydrogen, gaseous helium, or a combination thereof. In some embodiments, the method of the preceding paragraph may comprise adding salt to the cell housing prior to transferring the one or more liquefied gas solvents into the cell housing. Additional aspects, alternatives and variations as would be apparent to persons of skill in the art are also disclosed herein and are specifically contemplated as included as part of the invention. The invention is set forth only in the claims as allowed by the patent office in this or related applications, and the following summary descriptions of certain examples are not in any way to limit, define or otherwise establish the scope of legal protection.

5.3 Detailed Description of the Invention

Reference is made herein to some specific examples of the present invention, including any best modes contemplated by the inventor for carrying out the invention. Examples of these specific embodiments are illustrated in the accompanying figures. While the invention is described in conjunction with these specific embodiments, it will be understood that it is not intended to limit the invention to the described or illustrated embodiments. To the contrary, it is intended to cover alternatives, modifications, and equivalents as may be included within the

spirit and scope of the invention as defined by the appended claims. In the following description, numerous specific details are set forth in order to provide a thorough understanding of the present invention. Particular example embodiments of the present invention may be implemented without some or all of these specific details. In other instances, process operations well known to persons of skill in the art have not been described in detail in order not to obscure unnecessarily the present invention. Various techniques and mechanisms of the present invention will sometimes be described in singular form for clarity. However, should be noted that some embodiments include multiple iterations of a technique or multiple mechanisms unless noted otherwise. Similarly, various steps of the methods shown and described herein are not necessarily performed in the order indicated, or performed at all in certain embodiments. Accordingly, some implementations of the methods discussed herein may include more or fewer steps than those shown or described. Further, the techniques and mechanisms of the present invention will sometimes describe a connection, relationship or communication between two or more entities. It should be noted that a connection or relationship between entities does not necessarily mean a direct, unimpeded connection, as a variety of other entities or processes may reside or occur between any two entities. Consequently, an indicated connection does not necessarily mean a direct, unimpeded connection unless otherwise noted. One embodiment relates to a cap design and electrolyte injection method in which a plug is used to reversibly create a seal in an energy storage device such as a battery or capacitor. The seal may be created as a function the differential pressure placed on the plug such that the plug opens when the pressure external the cell device housing is greater than the pressure internal to the housing. A liquefied gas solvent or liquefied gas electrolyte may be injected into a device and the plug creates an immediate seal when the differential pressure is near zero and when flow of liquefied

gas solvent or electrolyte is ceased. Further, the plug may itself be housed inside a smaller metal housing which is inserted into the cap. This metal housing may itself be used as an electrical contact to either the positive or negative electrode. Examples of the electrochemical energy storage device are described in International Patent Application Publication Nos . WO 2015/074006 (PCT / US2014 / 066015) and WO 2017/204984 (PCT / US2017 / 029821) , which are incorporated by reference in their entireties. In some processes, vacuum is pulled on the internal housing containing cell components prior to liquefied gas solvent or liquefied gas electrolyte fill to remove any gas from the cell. This may be done by mechanically holding the plug in an open state during vacuum. In some processes, a temperature differential between liquefied gas solvent or electrolyte to create a pressure differential due to the vapor pressure difference at the different temperatures is used to fill a cell. This can be done by holding the liquefied gas solvent or electrolyte at room temperature and lowering cell or device temperature to around + 10 °C. , around 0 °C. , around -10 °C. , around -20 °C. , around -30 °C. , around -40 °C. , around -50 °C. , around -60 °C. , around -70 °C. , or around -80 °C. Alternatively, the temperature of the liquefied gas solvent or electrolyte may be increased to around + 25 °C. , around + 30 °C. , around + 35 °C. , around + 40 °C. , around + 45 °C. and holding the cell at room temperature. Alternatively, the temperature of the liquefied gas solvent or electrolyte may be increased and cell to be filled temperature decreased. As used herein, one of skill in the art will understand the temperature differential refers to a difference in temperature between the cell and liquefied gas solvent source, such as a compressed gas cylinder. As used herein, one of skill in the art will under stand the pressure differential refers to a difference in pressure between the cell and liquefied gas solvent source, such as a compressed gas cylinder, created by the vapor pressure of the liquefied gas solvent or liquefied gas electrolyte or an externally applied pressure.

One of skill in the art will understand that the vapor pressure of the liquefied gas solvent or liquefied gas electrolyte may vary according to temperature, and so a combination of both temperature and pressure differential may be used to fill a cell. In some processes, an external pressure source to force the liquefied gas solvent or liquefied gas electrolyte through the mass transfer tube and into the cell is used. An external pressure may come from a variety of gasses such as argon, nitrogen, oxygen, carbon dioxide, hydrogen, helium, amongst others. The pressure used to force the material through the mass transfer tube should be greater than that of the vapor pressure of the material at the process temperature. Ideally, pressure should be around 1 psi, around 5 psi, around 10 psi, around 20 psi, around 30 psi, around 50 psi, around 100 psi, around 200 psi, or around 300 psi greater than the vapor pressure. In some embodiments, the liquefied gas solvent is capable of being placed under a compressive pressure equal to, or greater than, the liquefied gas solvent's vapor pressure at a temperature when the compressive pressure is applied, thereby keeping the liquefied gas solvent in a liquid phase. In some embodiments, the liquefied gas solvent has a vapor pressure above an atmospheric pressure of 100 kPa at a room temperature of 293.15 K.

In some embodiments, the liquefied gas solvent comprises one or more materials selected from the group consisting of fluoromethane, difluoromethane, sulfuryl fluoride, thionyl fluoride, carbon dioxide, methyl ether, 1,1 difluoroethane, chloromethane, and a combination thereof. In some embodiments, the liquefied gas solvent comprises fluoromethane and carbon dioxide. In some embodiments, the liquefied gas solvent comprises fluoromethane and sulfuryl fluoride. In some embodiments, the liquefied gas solvent comprises fluoromethane, sulfuryl fluoride, and carbon dioxide. In some embodiments, the ratio of sulfuryl fluoride to fluoromethane is lower than 1 : 9. In some embodiments, the ratio of sulfuryl fluoride to carbon

dioxide is about 1 : 1. A check valve which is used on the cell cap may take several configurations. In one embodiment, the check valve has an independent housing which may be inserted into a cap. The mechanism within the check valve housing may or may not be biased or spring operated. The seal within the check valve may be made by rubber on rubber contact, metal on rubber contact or metal to metal contact. The check valve housing and the material in which it is inserted may each be metallic or electrically insulating. The valve may be held mechanically in the cap by interference fit, welding, solder, brazing, epoxy, glass to metal seal or other suitable method known in the art. The location of the check valve maybe be located anywhere within the cap, but most preferably in the center, and oriented for gas flow in any direction, but most preferably vertically oriented along the cell's length. With reference to the outside of the cell housing, the top of the valve may also be flat with the top of the cap, but could also extrude above the cap surface for easy electrical contact or be embedded below the cap surface such that the top of the valve is below the top of the cap. In order to ensure high integrity of sealing the high pressure liquefied gas solvent or liquefied gas electrolyte within the cell, an additional plug may be added to the top of the check valve. This plug may be welded, soldered, or press fit to ensure seal. With reference to the inside of the cell housing, the valve may flat with the bottom of the cap, extrude out further than the bottom of the cap, or have the valve bottom higher than the cap bottom. In one embodiment, the valve bottom extends further than cap bottom and into the mandrel diameter of the electrode winding, which will allow gas to flow preferentially down the center of the electrode winding. Electrical contact from either the negative or positive electrode may be made directly to the valve such that it may be used as a current collector contact and contacted from outside the cell to make electrical contact to the electrode. In Figure 5.1a-c , the check valve is held in place by a press fit. Figure 5.1a features a press fit into a metallic

component. The metallic component is also mechanically held in place via interference fit with electrically insulating component. A component is also placed on top of the cap to weld to the can edge to further improve mechanical rigidity. O-ring components and are also used to eliminate leak paths through interference fit pathways. In this embodiment, electrical conduction to one of the electrodes may be through or. Further, Figure 5.1b features the check valve insert into an electrically insulating component. In this scenario, electrical conduction to one of the electrodes may be made directly through a metallic check valve housing.

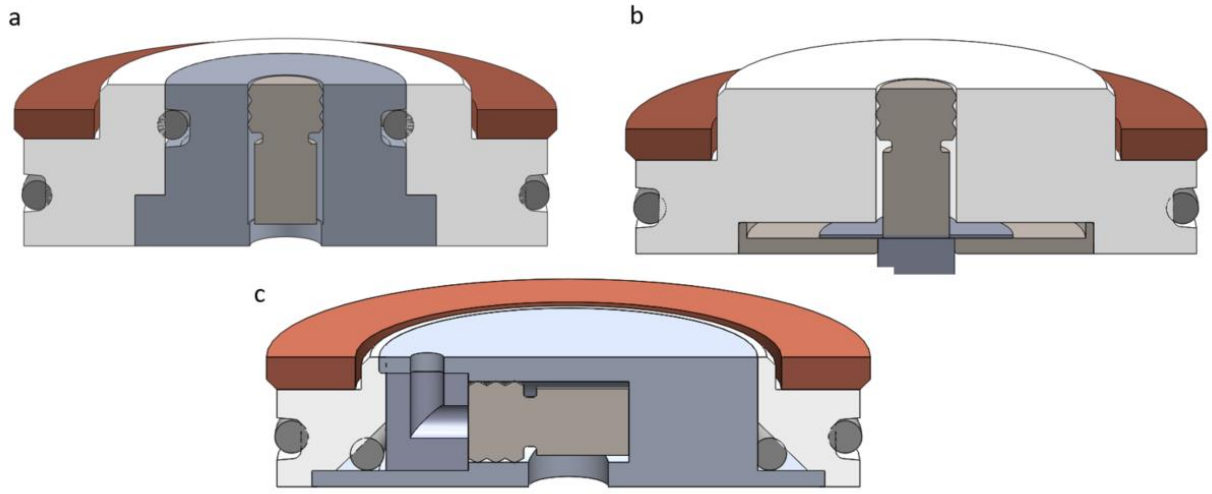

Figure 5.1 The cross-section view of one possible embodiment of the mechanical constructions of a cell cap.

Figure 5.1a shows a press fit into a metallic component. Figure 5.1b shows the check valve inserted into an electrically insulating component. Figure 5.1c shows a check valve inserted horizontally into a cap according to one embodiment. Further, Figure 5.1c features a check valve which is inserted horizontally into the cap into component. After insertion, the valve is held in place by component. The cap features an overall lower height than cap designs featured in Figure 5.1a, b. Further, it is much more difficult to eject the check valve from cap due to high pressures built up within the cell housing. In another embodiment, the check valve is built into

the cap housing itself as shown in Figure 5.2a-b. In this example, a rubber or metal ball is housed in a metal housing which has an interference fit to electrically insulating component. There is also a mesh screen which supports the ball from falling out from the cap housing and a mesh support. When external pressure is greater than internal housing pressure, the ball may open a pathway for mass transfer as shown in Figure 5.2a. When the internal housing pressure is greater than the external pressure, the ball may close the pathway for mass transfer as shown in Figure 5.2b. The additional metal component may be used to weld or solder the crimped can walls to prevent the internal pressure from pushing the cap out of can. In some embodiments, the check valve is fluidly connected to an area of the housing and allowing the liquefied gas solvent or electrolyte to flow into the housing and preventing the liquefied gas solvent or electrolyte from flowing out of the housing.

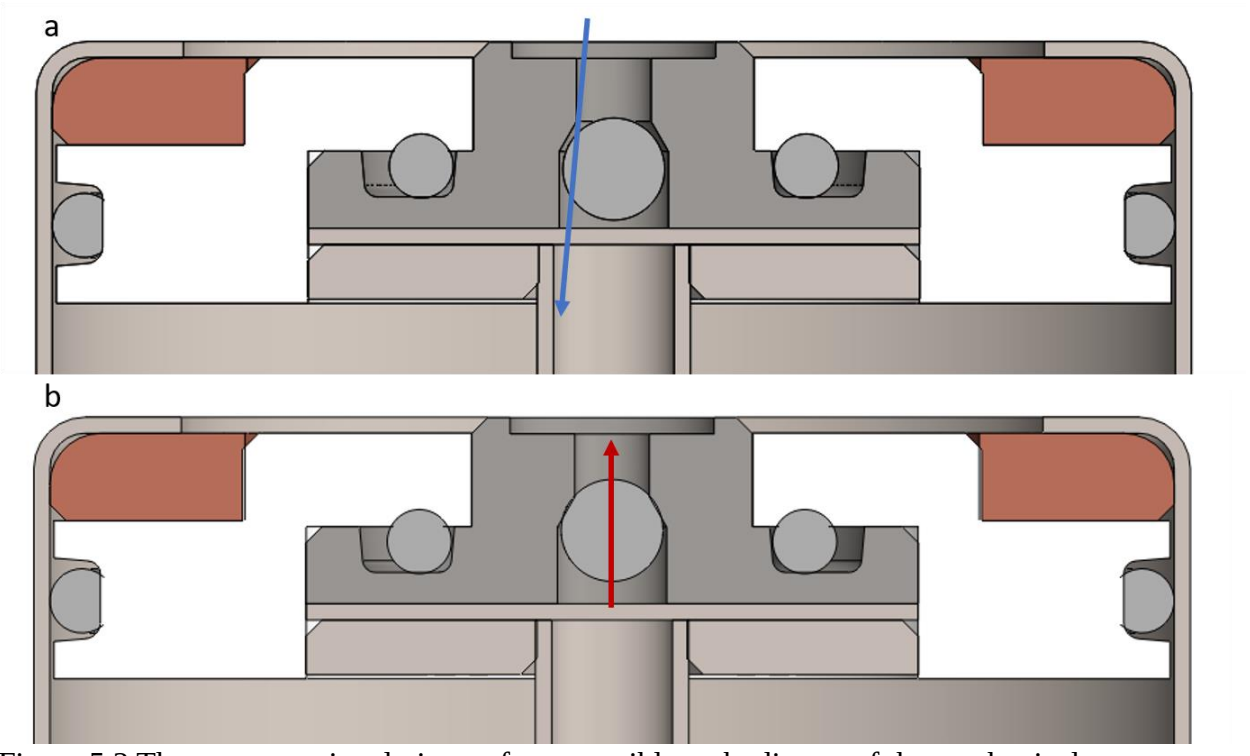

Figure 5.2 The cross-sectional views of one possible embodiment of the mechanical constructions of a cell cap.

In this design a check valve based on a ball is housed directly into the cap housing. In Figure 5.2a, the ball may open a pathway for mass transfer. However, as shown in Figure 5.2b, when the internal housing pressure is greater than the external pressure, the ball may close the pathway for mass transfer. In another embodiment, the cap may feature a valve built into the cap 1 which uses a spring to create a minimum differential pressure in order to open the valve and allow mass transfer, as shown in Figure 5.3. In this example, there is a greater surface area to make a seal due to the non-circular rubber component geometry.

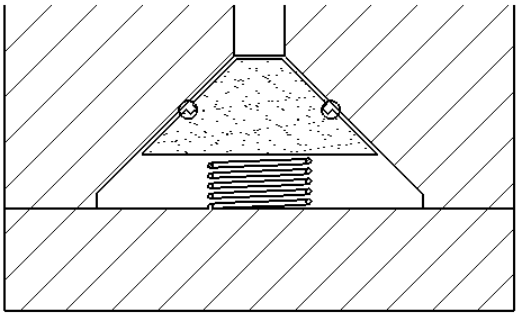

Figure 5.3 The cross-section view of one possible embodiment of the mechanical constructions of a cell cap.

In this design a check valve using a spring creates a minimum differential pressure to seal the cap. Figure 5.4 shows a plot of mass vs time of an example cell which was constructed using a geometry similar to Figure 5.2. At day 0, the cell was empty of liquefied gas solvent and at day 1 the cells were filled with solvent using a differential pressure method and check valve. The mass increased by approximately 3 grams for two example cells. The mass held fairly constant over several days showing the very good seal on the check valve and rest of cap seals. An electrochemical cell was built with a cap design similar to Figure 5.2 and with battery type electrodes. A salt was preloaded into the cell device and liquefied gas solvent was mass transferred into a cooled cell as a gas and liquefied within the cell due to the pressure within the

housing being higher than the vapor pressure of the solvent at the cell housing temperature. The solvent mass transfer went through the check valve in the cap and sealed shut after fill. After liquefying inside the cell, the solvent mixes with the salt in the cell to form a liquefied gas electrolyte.

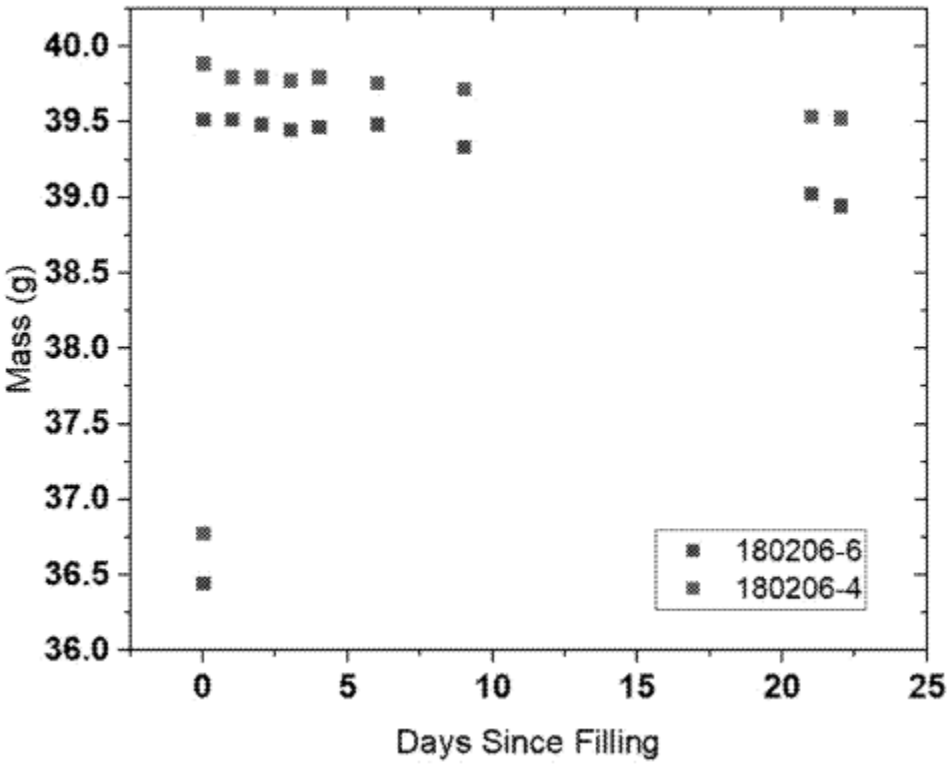

Figure 5.4 A plot showing the change of mass over number of days of two representative cells before and after liquefied gas filling and sealing.

An impedance spectrum of this cell is shown in Figure 5.5, showing a functional cell. Electrical connection to one electrode was made through the check valve metal component which electrical connection to the other electrode was made through the cell metal housing.

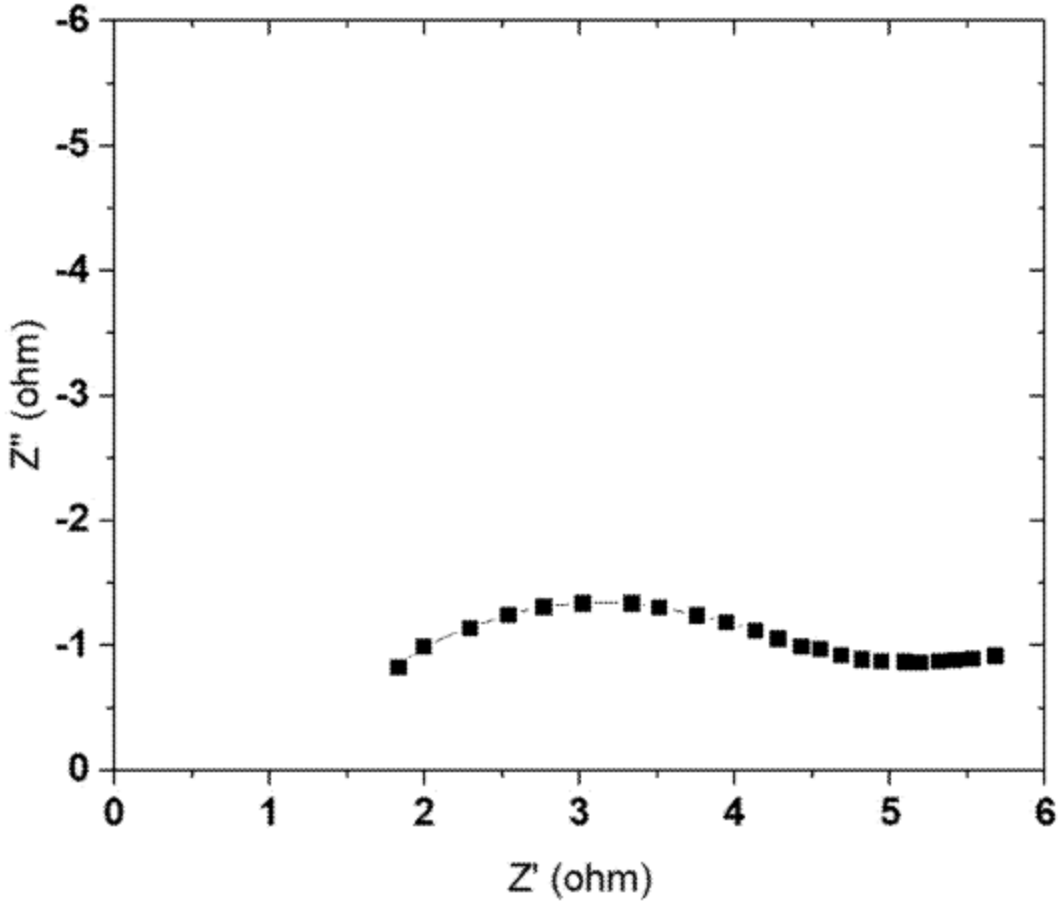

Figure 5.5 An impedance spectra of an exemplified cell after filling with liquefied gas solvent.

Although exemplary embodiments and applications of the invention have been described herein including as described above and shown in the included example Figures, there is no intention that the invention be limited to these exemplary embodiments and applications or to the manner in which the exemplary embodiments and applications operate or are described herein. Indeed, many variations and modifications to the exemplary embodiments are possible as would be apparent to a person of ordinary skill in the art. The invention may include any device, structure, method, or functionality, as long as the resulting device, system or method falls within the scope of one of the claims that are allowed by the patent office based on this or any related patent application.

1. An electrochemical device , comprising : a cell housing, two or more electrodes, an electrolyte comprising a liquefied gas solvent, and a cap with a check valve, wherein the check valve is configured to seal shut under higher internal cell pressure compared to outside cell pressure.

2. The electrochemical device of claim 1, wherein the electrochemical device comprises a cap housing that is independent from the cell housing.

3. The electrochemical device of claim 2, wherein the check valve is built into the cap housing.

4. The electrochemical device of any one of claim 1, wherein the check valve acts as an electrical contact to one of the two or more electrodes.

5. The electrochemical device of any one of claim 1, wherein the check valve comprises a spring configured to create a minimum differential pressure.

6. The electrochemical device of any one of claim 1, further comprising a plug or seal connected to the top of the check valve.

7. The electrochemical device of claim 6, wherein the plug or seal is soldered, welded or pressed fit onto the top of the check valve.

8. The electrochemical device of claim 1, wherein the liquefied gas solvent is capable of being placed under a compressive pressure equal to, or greater than, the liquefied gas solvent's vapor pressure at a temperature when the compressive pressure is applied, thereby keeping the liquefied gas solvent in a liquid phase.

9. The electrochemical device of claim 8, wherein the liquefied gas solvent has a vapor pressure above an atmospheric pressure of 100 kPa at a room temperature of 293.15 K.

10. The electrochemical device of any one of claim 1, wherein the liquefied gas solvent is

selected from the group consisting of: fluoromethane, difluoromethane, sulfuryl fluoride, sulfuryl chloride, carbon dioxide, 1,1- difluoroethane, chloromethane, and a combination thereof.

11. A method of preparing an electrochemical device of any one of claim 1, comprising transferring the liquefied gas solvent into the cell housing by connecting the liquefied gas solvent to the check valve and building a pressure differential between the interior and exterior of the cell housing.

12. The method of claim 11, wherein the pressure differential is created by a temperature differential inside and outside of the cell housing.

13. The method of claim 1 , wherein the pressure differential is created by introduction of gaseous argon, gaseous nitrogen, gaseous oxygen, gaseous carbon dioxide, gaseous hydrogen, gaseous helium, or a combination thereof into the cell housing.

14. The method of any one of claim 11, further comprising adding salt to the cell housing prior to transferring the one or more liquefied gas solvents into the cell housing.

Chapter 5, in full, is a reprint of the patent application “Electrochemical Cell Cap for Liquefied Gas Electrolyte” as it appears in US Patent App. 16/666,131, C.S. Rustomji, Y. Yang, D. M. Davies, J. Lee, Y.S. Meng. The dissertation author was primary investigator and first author of the patent application.

Chapter 6. A Safer, Wide Temperature Liquefied Gas Electrolyte Based on Difluoromethane

6.1 Introduction

Batteries are ubiquitous today in a huge number of applications. They vary greatly in size and application, from portable electronics to providing energy storage for grid reliability and resiliency. The front running chemistry for a number of these applications is the intercalation-based Li-ion battery, which has received a great deal of attention in the last few decades[10,53,54]. Scientists are nearing the theoretical limits of conventional (graphite-based anode) intercalation chemistries[55]; however, there is still a demand for next-generation batteries with higher energy density to meet expanding needs. Using Li-metal as the anode has been touted as the next great step in producing batteries with higher energy densities[56]. This is primarily due to Li-metal's much higher theoretical capacity density than that of graphite. Further, it provides a Li source, which opens the possibility of using cathodes that do not provide their own Li, including promising cathode systems such as sulfur or oxygen[57]; however, adoption of rechargeable Li-metal batteries has been limited due to low Coulombic efficiencies (CEs), dendrite growth, large volume change during cycling[58], and safety concerns.

Recently, electrolyte development has received a lot of attention as a possible pathway to achieving stable Li-metal interfaces and cell performances. However, researchers also need to consider the safety and the operation temperature and power of the electrolytes in order to expand the boundaries of practical, high-energy density batteries. Although conventional carbonate-based electrolytes have high oxidation stability (4.3 V vs. Li)[11,] they display poor compatibility with Li-metal anodes and are known to be highly flammable[59]. Ether-based

electrolytes cycle with relatively high CEs; however, their use is limited by low oxidation stability (<4.0 V vs. Li)[12]. Low molecular weight ethers are also highly flammable.

More recently, high-concentration electrolytes have been shown to form LiF-rich SEIs through salt decomposition. and high CE cycling of Li-metal has been demonstrated with these electrolytes. Further advances in this field have brought about locally highly-concentrated electrolytes which partially mitigate some of the disadvantages of highly-concentrated electrolytes – namely their cost, viscosity, wettability, and poor performance at low temperatures[13]. In addition, in recent years there has been a large amount of interest in solid-state electrolytes (SSEs) for Li-metal based batteries; however, these electrolytes also have been hindered by low conductivity at low (and even ambient) temperatures[14].

Along with the focus on both liquid and solid electrolytes, lately there have been developments with solvents that are gaseous at ambient temperature and pressure [60,61]. At moderate pressures or low temperatures these gaseous molecules can be liquefied, functioning as solvents that can dissolve Li salts to form liquefied gas electrolytes (LGEs). In these articles, successful cycling of Li-metal using fluoromethane (CH_3F, FM)–based electrolytes with dendrite-free morphology and high CE has been presented. The low melting point, low viscosity, inherent pressure, electrochemical stability, and high donatable fluorine content [62] combine synergistically to enable excellent Li-metal performance, even down to temperatures as low as -60 ℃. However, there has been uneasiness about the practicality and safety of LGEs. Along with worries about the manufacturability of batteries utilizing LGEs, the three factors of most concern are the inherently high internal pressure, flammability, and low critical point of the solvent.

Here, we demonstrate results and progress towards alleviating concerns regarding the practicality and safety of using LGEs. First, we present an enhanced safety feature inherent in

LGEs by showing the results of a nail-penetration test on a full Li-ion cell in an 18650 form-factor cycled with an LGE. Next, we demonstrate the potential of using LGEs with difluoromethane (CH_2F_2, DFM) as the primary solvent, which exhibits improved safety features and operational temperature range. We use computational and spectroscopic techniques to help understand the solvation and transport of the system. The electrolyte shows impressive conductivity between -60 and +70 ℃ and compatibility with both the Li Metal anode and the 4 V class NMC cathode. By demonstrating this enhanced safety feature and the viability of using a low-flammable solvent, we lower the barriers of adoption for developing safe and practical LGEs.

6.2 Materials and Methods

6.2.1 Materials

The salts Lithium bis(fluorosulfonyl)imide (LiFSI) (99.9%) and lithium bis(trifluoromethane)sulfonimide (LiTFSI) (99.9%) were obtained from BASF. Fluoromethane (99.99%) and Difluoromethane (99.99%) were purchased from commercial sources. 1,2-dimethoxyethane (DME, 99.5%), and 99.8%) were purchased from Sigma-Aldrich and stored over molecular sieves. The NMC622 (A-C023) was obtained from Argonne national laboratory. The $LiFePO_4$ was purchased from MTI.

6.2.2 Electrochemical Measurements

Electrolytic conductivity measurements were performed in custom fabricated high-pressure stainless-steel coin cells, using polished stainless-steel (SS 316L) as both electrodes. The cell constant was calibrated from 0.447 to 80 $mS \cdot cm^{-1}$ by using OAKTON standard

conductivity solutions. Battery cycling tests were performed by an Arbin battery test station (BT2043, Arbin Instruments, USA) in custom designed high-pressure stainless-steel coin cells, with Li metal (FMC Lithium, 1 mm thickness, ¼ inch diameter) as the counter electrode and Cu foil as the working electrode. A single 25μm porous polypropylene separator (Celgard 2075) was applied for all the electrochemical experiments. For Li metal plating and stripping experiments, Li was first deposited onto the working electrode at 0.5 $mA \cdot cm^{-2}$ until 0 V vs. Li and the voltage was held for 5 hours to form a stable SEI on the current collector. The first plating cycle was then started, followed by complete Li stripping to a 1 V vs. Li cut off voltage. The CE was calculated as the Li stripping capacity divided by the Li plating capacity during a single cycle. For the tests at different temperatures, the cells were stored at the testing temperature in a temperature chamber (Espec) for several hours before cycling. In Li-NMC cycling, the cell was firstly cycled at C/10 rate at room temperature for 2 activation cycles and were subsequently cycled at selected rates and temperatures.

6.2.3 Electrolyte Addition

Electrolyte addition procedures have been described previously.[60]

6.2.4 Material Characterization

Raman spectra of liquefied gas electrolytes were carried on Renishaw inVia confocal Raman microscope with an excitation wavelength of 532 nm. All spectra were calibrated with Si (520 nm) and analyzed by Wire 3.4 software developed by Renishaw Ltd.

6.2.5 Computational Methods

Molecular dynamics simulations were performed using APPLE&P polarizable force fields[23,63]. The LiFSI and DME force field parameters accurately predicted structure and transport properties of the similar DME-LiTFSI and DME-DOL-LiTFSI electrolytes. [64] The Li^+/DFM parameters were developed in this work following previously described methodology by fitting to quantum chemistry data. [65] Charges were fit to electrostatic potential calculated around DFM at the MP2/aug-cc-pvTz level, yielding DFM dipole moment of 2.12 Debye vs. 2.0 D from MP2/aug-cc-pvTz quantum chemistry calculations. DFM molecular polarizability was 2.5 $Å^3$ from force field and 2.51 $Å^3$ from M05-2X/aug-cc-pvTz DFT calculations. Molecular mechanics calculations using developed force field yielded the Li^+/DFM binding energy -25.2 kcal/mol in good agreement with the a value of -25.0 kcal/mol from G4MP2 quantum chemistry calculations.

Two systems were simulated. One system was composed of 120 LiFSI, 156 DME, and 1960 DFM molecules corresponding to the 1 M LiFSI, 1.3 M DME in DFM electrolyte. The other system was composed of 32 LiFSI, 38 DME, and 1960 DFM molecules corresponding to the 0.3 M LiFSI, 0.35 M DME in DFM electrolyte. Two replicas were created, and simulations for each replica were started from different levels of aggregation in the electrolytes. Equilibration runs were 20-170 ns followed by 20-140 ns production runs for all simulated systems (**Table S3**). Multiple timestep integration was employed with timestep of 0.5 fs for bonded interactions, time step of 1.5 fs for all non-bonded interactions within a truncation distance of 8.0 Å and an outer timestep of 3.0 fs for all non-bonded interactions between 8.0 Å and the nonbonded truncation distance of 18 Å. The Ewald summation method was used for the electrostatic interactions between permanent charges with permanent charges or induced dipole moments with $k = 7^3$ vectors. The reciprocal part of Ewald was calculated every 3.0 fs. Induced dipoles were found

self-consistently with convergence criteria of 10^{-9} (electron charge * Å)^2.

6.3 Inherent Safety Feature of Liquefied Gas Electrolyte

The nail penetration test has been widely used by battery companies, automotive manufacturers, and other battery users[66]. This test involves driving a nail through the battery, consequently creating a short circuit. In conventional Li-ion batteries, the short circuit in this test typically results in heating of the battery, often leading to thermal runaway, with the battery generally displaying smoke, fire, or even exploding shortly after the nail penetration[67]. Such tests are typically conducted on batteries in conventional, practical form factors such as pouch or cylindrical cells. It has been shown that the likelihood of a battery undergoing a thermal event is substantially increased when the nail penetration location is central and the battery is at a high state of charge[68].

To test the effects that the different physio-chemical properties of LGEs would have on the nail penetration test, we used a battery containing conventional electrode materials (Graphite Anode, Lithium Nickle Manganese Cobalt Oxide (Li_1 $Ni_{1/3}$ $Mn_{1/3}$ $Co_{1/3}$ O_2) Cathode) in a cylindrical 18650 format. Using a custom designed cap[69] and electrolyte insertion process we filled the cell with an LGE - 0.3 M Lithium bis(trifluoromethanesulfonyl)imide (LiTFSI), 0.3 M tetrahydrofuran (THF), in 19:1 FM:CO_2. The 18650 cell underwent three full cycles and was fully charged to 4.2 V, before nail penetration was performed in the center (horizontal axis) of the jelly roll.

The results of the nail penetration test are displayed in Figure 6.1. The approximate time of penetration during the test is indicated by the sharp decrease in cell voltage to 0 V. During nail penetration with the LGE, two interesting things happened. First, immediately after penetration

the non-toxic solvent rapidly evaporated and escaped. This is supported by the temperature profile seen in the nail penetration results. In conventional Li-ion batteries with liquid electrolytes, after nail penetration, the temperature of the cell often rises rapidly. In contrast, in our system containing an LGE, during the penetration we saw a sharp decrease in the temperature of the cell to below -10 ℃ due to the cooling effect of the swiftly expanding gas escaping from the cell. The cell temperature then stabilized back to approximately room temperature and no sparks or flames were observed throughout the test. The second, less obvious effect, was that the ionic conductive pathway was eliminated as a result of the gas dissipating. Once the bulk solvent had been removed, there no longer was a medium in which the Li-ions could freely move between the electrodes, and consequently the ionic transport and short-circuiting of the battery was prevented. This behavior is characteristic of LGEs due to their inherently high volatility and results in a distinctive safety feature unique to this class of electrolytes. Regardless of whether the primary solvent is FM or another liquefied gas, the effect will be present in solvents with sufficiently high volatility. Similarly, under other physical abuse such as over-charge or high temperature exposure, the cell may avoid thermal runaway by safely venting.

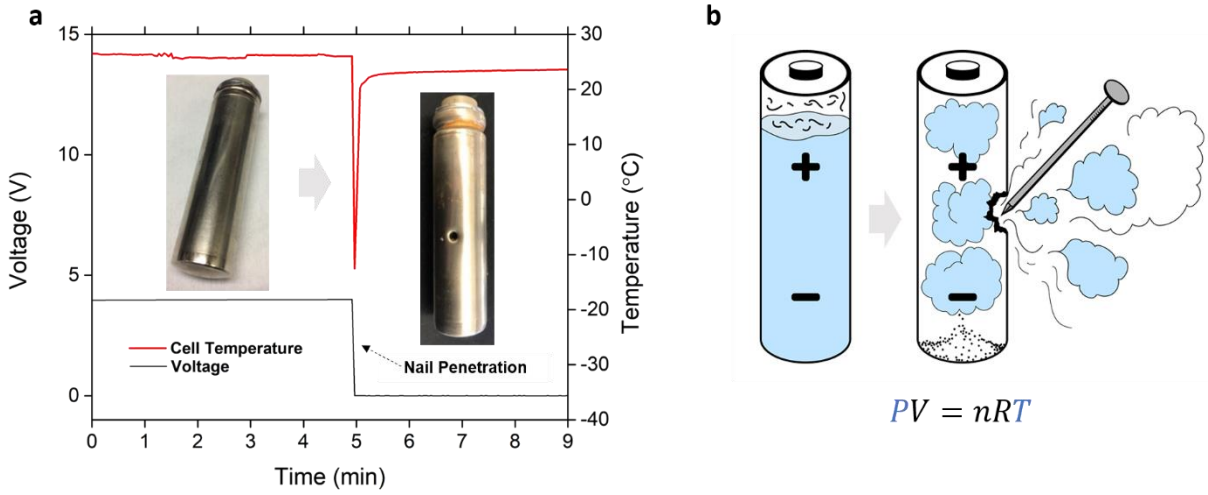

Figure 6.1 Nail Penetration of an 18650 Form-Factor Cell with Liquefied Gas Electrolyte. (a) The voltage (black) and cell temperature (red) during a nail penetration test of a Graphite-NMC Li-ion battery in an 18650 form-factor filled with an LGE. The inset images show an 18650 cell before and after penetration. (b) schematic of the liquefied gas evaporating and expanding after nail penetration. The cell cooling is a direct result of the Ideal Gas Law. Salt remains in the cell.

6.4 Liquefied Gas Based on Difluoromethane

The low-melting point, low viscosity, wide electro-chemical stability window and high presence of fluorine are properties of FM that have combined synergistically to give impressive performance of electrolytes based on this solvent[14,15,21]. DFM maintains many of the beneficial properties of FM, including the low-melting point, low-viscosity, and relatively high dielectric constant. Figure 6.2a shows a comparison between some of the other important physical-chemical properties of FM and DFM. Notably, at +20 ℃, the vapor pressure of DFM (14.6 atm) is less than half that of FM (33.6 atm). Additionally, the critical temperature of DFM (+78.5 ℃) is significantly higher than that of FM (+44.5 ℃)[70]. As is shown previously [60,71], this value is important for the high temperature conductivity of LGEs, especially with low salt concentrations. The table also shows interesting properties regarding the flammability of the two substances which are detailed below.

The American Society of Heating, Refrigerating and Air-Conditioning Engineers

(ASHRAE) standard 34 (ISO 817:2014) classifies the flammability of a refrigerant in 4 different categories: 1 (non-flammable), 2L (low flammability), 2 (flammable), and 3 (high flammability)[72,73]with the prefix "A" indicating that the solvent is non-toxic. Likely due to a small worldwide usage in refrigeration applications, FM does not have an official ASHRAE classification. Given its heat of combustion (19.8 MJ kg^{-1})[74], lower flammability limit 5.6 (v/v %)[26], and laminar burn velocity (28.2 cm/s) [74], it is predicted that it would be classified into group A3[75].

On the other hand, DFM is widely used as a refrigerant[76] and has been assigned the designation A2L – reserved for low toxicity refrigerants that are difficult to ignite or sustain a flame [72]. The class 2L is distinguished from 2 by the requirement that the laminar burning velocity of the refrigerant must be below 10 cm/s. With its low laminar burn rate (6.2 cm/s)[77], low heat of combustion (9.4 MJ kg^{-1}) [78],and its relatively high flammability limit (14.4%)[79] DFM is increasingly being used as a refrigerant worldwide – both in blends, and is being explored as stand-alone option[32]. It is important to note here that conventional electrolytes such as $LiPF_6$ salt in mixtures of ethylene carbonate and dimethyl carbonate solvents are highly flammable and pose other significant safety risks[80].The possibility of using low flammability solvents, combined with the inherent safety features of LGEs provide an unexpected pathway towards high performing, safe electrolytes.

a

Property	Fluromethane	Difluoromethane
Chemical Structure		
Vapor Pressure @ 20°C (atm)	33.6	14.6
Critical Temperature (°C)	44.5	78.5
Lower Flammability Limit (v/v %)	5.6	14.4
Upper Flammability Limit (v/v %)	22.2	33
Maximum Burn Velocity ($cm \cdot s^{-1}$)	28.2	6.7
Heat of Combustion ($MJ \cdot kg^{-1}$)	19.8	9.4
GWP 100	116	677

b

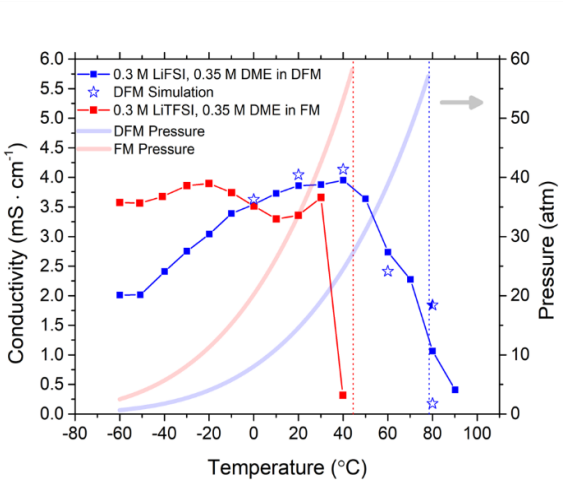

Figure 6.2 Physical-chemical properties of fluoromethane and difluoromethane (a) comparison of the physical-chemical properties of Fluoromethane and Difluoromethane. In the chemical structure the hydrogen is white, carbon is grey, and fluorine is green. GWP100 is an indication of how much energy is absorbed by the greenhouse gas over 100 years relative to CO_2 [24–27,29–31,34] (b) The conductivity of 0.3 M LiTFSI, 0.35 M DME in FM (red scatter & line) and 0.3 M LFSI, 0.35 M DME in DFM (blue scatter & line). The blue stars show the predicted conductivity from simulations of the DFM-based electrolyte. The half colored blue star indicates the simulation was run with higher compression. The partially transparent lines show how the vapor pressure of the solvents – FM (red), DFM (blue) vary with temperature. The dotted lines show the critical temperatures of the solvents – FM (red), DFM (blue).

Due to these advantageous properties of DFM, the reader may question why previous efforts with LGEs have focused on FM rather than DFM. This is because the solubilities of Li salts are generally lower in DFM than FM[13]. Recently, use of co-solvents (at ratios near 1:1 – co-solvent:salt), have been used to further improve the solubility of FM-based LGEs[71,81]. A similar approach is expected to improve the solubility of Li salts in DFM. A systematic study was conducted using a variety of salts, co-solvents and concentrations to try to identify the most promising LGE candidates. We found that at 1:1 ratios of co-solvent to salt, both LiTFSI and Lithium bis(fluorosulfonyl)imide (LiFSI) were unable to fully dissolve in DFM. By slightly increasing the ratio of co-solvent to salt, we were able to fully dissolve both LiTFSI and LiFSI salts. It is important to note that although in some cases there is twice as much co-solvent as salt on a molar basis, these systems would still qualify as “locally highly concentrated” electrolytes[82].

By using a low ratio of co-solvent:salt it is believed that the co-solvent is more likely to become fully coordinated by the salt, increasing its resistance to oxidation.[83] After creating and performing preliminary electrochemical testing on a number of electrolytes we decided to explore in detail systems using 1,2 dimethoxymethane (DME) as the co-solvent, and LiFSI as the salt. This LGE system was further studied as the DFM-based system since the co-solvent:salt ratio required to dissolve the salt was small and the systems yielded promising electrochemical performance, which is further detailed in a later section (Figure 6.4).

Figure 6.2b shows a comparison of the conductivities of electrolytes based on FM and DFM through wide temperature ranges, as well as the corresponding vapor pressures of the primary solvents in the respective temperature range. For the FM-based electrolyte, we see high conductivity (> 3 $mS \cdot m^{-1}$) from -60 to +30 ℃, followed by a drop in conductivity at +40 ℃ (near the critical point of the electrolyte) consistent with previous results[71,81]. The DFM based electrolyte has a similarly high conductivity at low temperatures (> 2 $mS \cdot cm^{-1}$) at -60 ℃, with a reduction in conductivity seen at the much higher temperature of approximately +70 ℃. This increased conductivity at high temperatures is attributed to the higher critical temperature of DFM than FM. As the electrolyte approaches the critical temperature, the amount of solvent in the liquid phase significantly reduces due to the increased density of the vapor phase. In the experimental conductivity setup used, it is believed that as this liquid volume is reduced, contact with the electrodes is not maintained, demonstrating a significant drop in conductivity.

6.5 Solvation and Transport Properties

Due to the pressurized nature of the LGE, it has previously been difficult to physically characterize the electrolytes. For this work, we developed a custom setup that allowed us to

perform Raman analysis on the pressurized electrolyte systems. The apparatuses are shown in Figure 3.2. To study the solvation structure, we added varying concentrations (0 M – 1 M) of LiFSI to 1.3M of DME in DFM. A concentration of 1.3 M DME was used (as opposed to 0.3 M) since the signal to noise of both the DME and FSI^- peaks were greatly enhanced using a larger amount of co-solvent and salt.

Figure 6.3a shows the peak characteristic of the C-O stretching vibration in the DME molecule. With 0 M of FSI^- (black line), this peak matches with the C-O stretching vibration seen in pure DME[84]. As more FSI^- is introduced, reduction in the normalized intensity of the free DME peak at 850 cm^{-1} occurs and a new peak arises at 874 cm^{-1}, which has previously been correlated with an increase in the coordination of DME to Li^+ [85]. At the highest concentrations of FSI^-, the C-O vibrational peak associated with free DME is no longer visible, indicating a strong degree of coordination between the DME and the Li^+. Figure 6.3b shows the characteristic peak of FSI^-. At low concentrations the peak is centered approximately around 725 cm^{-1}, which is consistent with previous literature[86]. With an increase in FSI^- concentration we see a shift in the characteristic peak to be centered around 750 cm^{-1}. This shift in the FSI^- peak has previously been attributed to an increase in aggregation of FSI^-, indicating a large amount salt aggregation in the electrolyte[40]. High aggregation has been shown in previous LGEs to lead to very few free FSI^- ions and subsequently a high transference number. Finally, Figure 6.3c shows the C-F stretching peak of DFM. We see that with increasing LiFSI concentration there is no shift of the peak from 527 cm^{-1}, but peak broadening is apparent. This indicates that very little DFM is coordinated with the Li ions in their first coordination shell, which is in contrast to the significant participation of FM in the first solvation shell of FM based systems [61]. These results indicate that the Li^+ is largely coordinated by DME, and FSI^-, forming substantial aggregates, with DFM

participating infrequently in the first solvation shell.

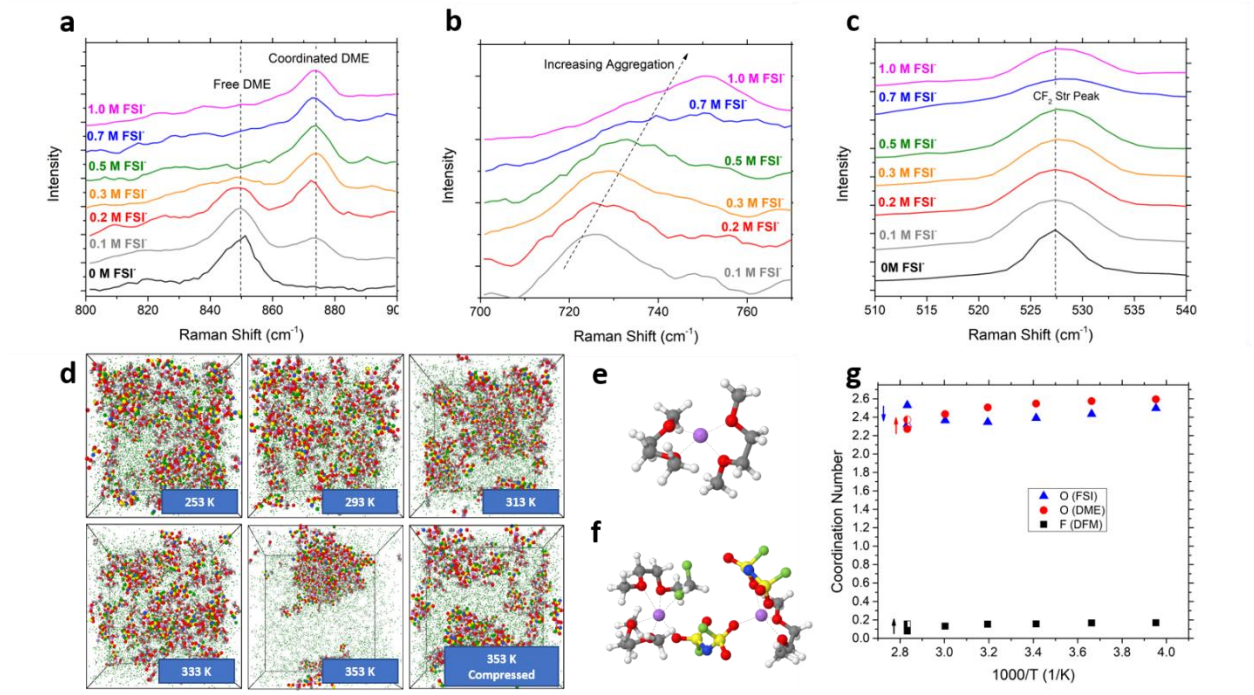

Figure 6.3 Spectroscopic and Characterization of the DFM-based electrolyte. (a-c) Raman spectra of LGEs with 1.3 M DME and increasing LiFSI concentrations in 800-900 cm^{-1} (DME C-O stretching peak), 700-790 cm^{-1} (LiFSI characteristic peak), and 510-540 cm^{-1} (DFM C-F stretching peak). (d) Snapshots of electrolyte systems at various temperatures. Size of DFM molecules lowered. (e, f) representative solvation structures of Li^+ from the simulations. (d) shows Li^+ surrounded by 2 DME molecules. (e) shows 2 Li^+ surrounded by 3 DME, 1 DFM, and 2 LiFSI molecules. (g) Coordination number of Li^+ at various temperatures. Lithium: purple, oxygen: red, carbon: grey, hydrogen: white, fluorine: green, nitrogen: blue, sulfur: yellow.

Molecular dynamics (MD) simulations were performed on the DFM-based electrolytes for two salt/co-solvent concentrations: 1M LiFSI, 1.3M DME in DFM and 0.3M LiFSI, 0.35M DME in DFM. We observed similar ion solvation trends and transport mechanisms for both salt concentrations and, therefore, focus our discussion only on the higher salt concentration for simplicity. Analysis of the Li^+ coordination via the radial distribution functions (RDFs) revealed

a strong preference for Li^+ coordination by the oxygen of DME, followed by the oxygen of the FSI^- and only week coordination with DFM fluorine atoms. Figure 6.3g shows a composition of the Li^+ first solvation shell (at 2.8 Å) at different temperatures. At room temperature, a Li^+ cation, on average, is coordinated to 2.5 O (DME) out of 2.6 available due to DME:Li=1.3 ratio, 2.4 O (FSI^-), and 0.16 F (DFM). This indicates that almost all the DME is coordinated to Li^+ and that DFM has little participation in the first solvation shell of Li^+, consistent with the Raman results shown in Figure 3a and Figure 3c. Figure 3e shows a representative solvate for a free Li^+, while Figure 3f shows a representation of an ionic aggregate. Representative snap shots of the simulation cell at different temperatures are shown in Figure 3d. In agreement with to the FM based electrolytes, we see an increase in aggregation with temperature[61,71]. This aggregation and disappearance of the solvent separated free ions contributes to the eventual conductivity loss of the electrolyte at high temperatures that is accurately predicted by MD simulations (see Figure 2b). Specifically, the degree of ion correlation (a_d) that is often called ionicity decreases with increasing temperature. This decrease partially compensates for the increase in diffusion coefficients of the molecules at lower temperatures (Figure S6) leading to the relatively flat conductivity curve through a wide temperature range. Note that in addition to MD simulations at the experimental densities, we performed MD simulations of a compressed electrolyte at +80 °C, having a density approximated from experiments at +60 °C. Electrolyte compression leads to an increase in ionization, free Li^+ cations and conductivity of the electrolyte. It is believed that the actual compression of the electrolyte is somewhere between the two methods used. Future work will focus on more accurate modelling of the electrolyte compression at temperatures near the critical point of liquefied gas solvent but will require even larger simulations cells with a larger number of ions to accurately capture large ion cluster formation.

6.6 Li-Metal Anode and Li-Metal Battery Performance

We explored the compatibility of the DFM-based electrolyte by conducting Li-metal plating/stripping tests on Cu electrodes. The SEI formed by DFM with Li, is more stable that the SEI formed by FM which eliminates the need to add carbon dioxide in the system. 0.3 M LiFSI, 0.35 M DME in DFM (Figure 6.4) was used as the DFM-based LGE for electrochemical studies. We also compared the results to a 1 M LiFSI in DME liquid electrolyte. With the DFM based LGE, we see a first cycle CE of 94.5% which increased to an average CE of 98.2% over 100 cycles (Figure 6.4a). The electrolyte demonstrates higher efficiency and better stability cycling of Li-metal than both the 0.3M LiFSI in DME (93.2%), and the more common 1M LiFSI in DME (97.1). In Figure 6.4b we see that stable cycling of Li-metal is possible between -40 and +55 ℃ with this LGE. The performance of the electrolyte at low temperatures is far superior to the conventional ether-based electrolyte, which shows unstable cycling at -20 ℃ and was unable to cycle at -40 ℃. After returning to room temperature, we see an average CE of over 100%, likely due to the release of Li+ ions previously held by the SEI layer back into the system[14]. Stable, high efficiency cycling is demonstrated at the raised temperature of +55 ℃, a temperature previously inaccessible by low-concentration FM-based LGEs. Representative voltage curves during cycling in the LGE are shown in Figure 6.4c, which show low, stable over-potentials down to -20^{O}C with a slight increase in overpotential at -40 ℃. Upon returning to +20 ℃ we see that the voltage curve is almost identical to what it was prior to the low and high temperature cycling. These initial results are promising, and future work will explore methods to further improve the CE through novel electrolyte design such as co-solvents, additives and new salts.

To explore the compatibility of the DFM based electrolyte with 4 V class cathodes, we

made full Li-metal cells using commercial LiNi0.6Mn0.2Co0.2O2 (NMC622) cathodes with capacity loading of ~1.8 mAh·cm^{-2}. Figure 6.4d shows promising wide-temperature, full cell cycling. For these results, the charging temperature was the same as the discharging temperature, therefore including the effects of limited charging kinetics at low temperature. Cycling in the range of -60 to +55 ℃ is demonstrated with 42% capacity retention at -40 ℃ (as compared to +20 ℃) and good performance shown up to +55 ℃.These results show the possibility to design safer LGEs based on alternative solvents to perform in high energy density batteries in wide temperature ranges.

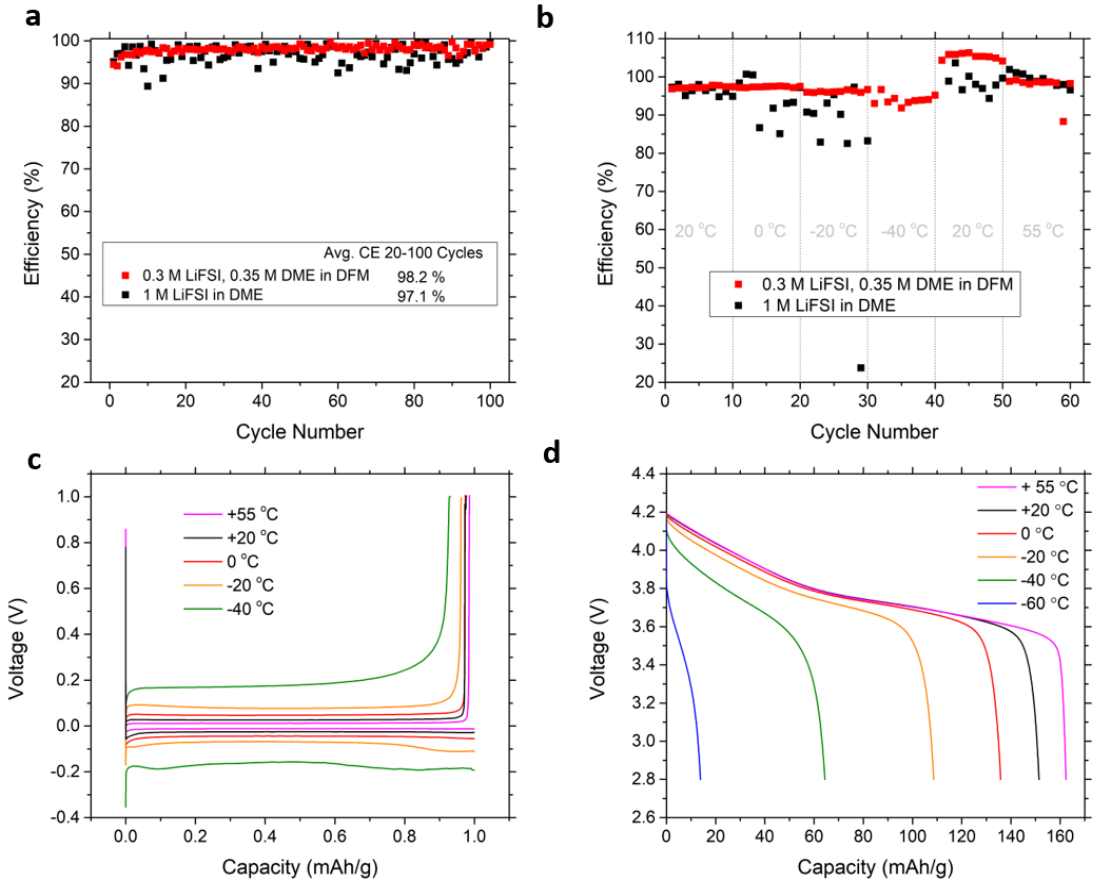

Figure 6.4 Electrochemical performance of the Li metal anode in the liquefied gas electrolyte in a wide temperature range. LGE used: 0.3 M LiFSI,0.35 M DME in DFM (a) The CE of Li metal plating/stripping over 100 cycles at 0.5 mA/cm^2,1.0 mAh/cm^2. LGE: red; 1 M LiFSI in DME:

black. (b) The CE of Li metal plating/stripping (at 0.5 mA/cm^2,1.0 mAh/cm^2) at various temperatures. LGE: red; 1 M LiFSI in DME: black (c) voltage profiles for the LGE cell in (b). (d) Li-NMC 622 cell cycled at a rate of C/20 at temperatures of +20℃, 0℃, -20℃, -40℃, -60℃, and then +55 ℃ with the LGE.

6.7 Conclusion

In this study we endeavored to quell some of the previous concerns raised about the safety and practicality of using liquefied gas-based electrolytes. First, we demonstrated impressive safety results with 18650 format cells containing LGEs, cooling rapidly under nail penetration. This phenomenon is inherent to the LGEs and is expected to be present in all systems containing these gases (whether the gas is FM, DFM or some other liquefied gas solvent). Next, we developed an LGE based on DFM as the primary solvent and identified a formulation that helps to mitigate some of the major issues that have arisen with LGEs based on FM. The new DFM-based electrolyte has a lower pressure, lower flammability, and a higher maximum operating temperature than its FM-based predecessors. Importantly, DFM still possesses many of the properties that make FM an attractive solvent, such as low viscosity and a wide electrochemical window. The electrolyte demonstrated good conductivity, as well as Li-metal and 4 V class cathode compatibility through a wide temperature range.

Conventional wisdom suggests that the gaseous nature of LGEs gives rise to significant battery system safety and practicality concerns. In this paper, however, we have shown that the pressurized nature of such LGE systems actually provides significant and unique safety benefits. By demonstrating the use of, and characterizing an LGE with an alternative, lower pressure, and low-flammability solvent, we also have shown a path forward to explore different LGEs and the potential for these systems to be used in safe and practical high energy density batteries.

Chapter 6, in full, is a reprint of the material “A Safer, Wide Temperature Liquefied Gas Electrolyte Based on Difluoromethane” by D. M. Davies, Y. Yang, E. S. Sablina, Y. Yin, M. Mayer, Y. Zhang, M. Olguin, J. Z. Lee, B. Lu, D. Damien, O. Borodin, C. S. Rustomji, and Y. S. Meng which is under review at Journal of Power Sources

Chapter 7. Summary and Outlook

Batteries are ubiquitous in today's society. With a multitude of chemistries and form-factors, they are used in a massive number of applications. As the world moves towards the use of more renewable energy, batteries will additionally play an increasingly crucial role in large scale energy storage, for example in transportation sectors (electric vehicles), and grid storage. The focus of my thesis was to present a multi-scale approach to this development, focused on grid-scale energy as well as next-generation Li batteries.

In Chapter 4, we used models of storage connected to the California energy grid and showed how the application-governed duty cycles (power profiles) of different applications affect different battery chemistries. A reliable understanding of the potential revenues obtainable by energy storage systems in different applications was provided. We also developed a technique for accurately measuring the performance of cell-level battery chemistries undergoing duty cycles representative of these applications. It is shown that in order to accurately predict the potential revenue of batteries on the grid the efficiencies of the devices must be considered for each different application they participate in. The differences in efficiency between chemistries and across applications alter the relative value of each battery chemistry in that application. This combined economic and technological evaluation could help to alter and improve the accuracy of how energy storage technologies are evaluated for grid-scale use.

Chapters 5 & 6 are focused on the development of liquefied gas electrolytes for next-generation batteries. Recently, liquefied gas electrolytes have shown to be promising candidates to enable Li-metal for next generation batteries, however, there have been concerns about the manufacturability and practicality. In these two chapters we further develop these systems to help

lower the barriers to adoption of this novel technology. Chapter 5 is more focused on the cell-scale mechanical development, presenting a method to fill, and seal, the liquefied gas electrolyte into a conventional 18650 cylindrical cell. This demonstrates the feasibility and manufacturability of cells utilizing liquefied gas electrolytes. Chapter 6 focuses on material (and atomic level) development, demonstrating the feasibility of using a liquefied gas electrolyte with lower flammability and pressure than previously used. A combination of Molecular Dynamics and Raman spectroscopy were used to characterize the electrolyte down to the molecular level. This section helps to quell concerns over the safety and practicality of using liquefied gas electrolytes.

For future work related to the economic modeling, there is a huge amount of work to be done, and a number of places to look to. First, I would suggest looking at scale. The experiments demonstrated in this thesis were focused on cell chemistry. Attention needs to be paid to both different form-factors, and larger scale systems. Especially regarding the inclusion of inverters and other power electronics. Second, the scope of the applications will constantly need to evolve, and also expand to other grids. The applications performed by batteries will change over time. This will potentially happen quite rapidly in the coming years as the amount of renewable generation and storage increases on the grids. Clearly, attention should also be paid to markets other than the California grid, with different states and countries having entirely different markets. In the short-term, focus could be placed on revenue generated by stacking applications together. Third, how the applications affect the lifetime of the electrochemical cells should also be tested and considered. This testing will require long-term cycling, but, if combined with revenue and cost analyses, would help immensely to gain insight into the optimal marriage of chemistry, form-factor, and application.

Future work related to the mechanical design of electrochemical cells utilizing liquefied gas electrolytes should (and has) been continued in industry. The proof of concept designs demonstrated in this thesis have paved the way for more advanced and automated (and more capital intensive!) techniques to be used. From an academic standpoint it would still be extremely interesting to use conventional form-factor cells (18650s) and to see the effect of high temperature (above the critical point of the electrolytes) on the conductivity and cyclability of the cells. Mechanical design focus should (and has) shifted in the academia towards designing and constructing housings for the advanced characterization of the electrolytes. This has already been demonstrated for techniques such as Raman and could easily be extending to infrared absorbance spectroscopy which is a complimentary technique. Electrolytes operating near their critical points is a relatively unexplored field and many advances in understanding could be made. The use of glass or windows in the electrochemical cells could easily help to provide insight into the true nature of the high temperature conductivity drops seen in the electrolytes. This could also be aided by more advanced pressure measurements of the electrolyte as well as density measurements of the liquid portion of the electrolyte.

As far as electrolyte development is concerned there are many different paths to explore. The first is to continue to develop the chemistry for different Li-metal and Anode-free applications. This could be done by exploring combinations of different salts, liquid co-solvents, and liquefied gas solvents and co-solvents. One obvious path to explore is to use mixtures of different liquefied gas solvents to make use of different beneficial properties. For example, a liquefied gas such as Fluoromethane or Dimethyl ether could be mixed with a flame retardant gas to ensure both good solubility and low flammability of the electrolyte. The most anticipated difficulty in using alternative liquefied gas cosolvents is to achieve sufficient solubility of the

salts, while maintaining sufficient miscibility with co-solvents.

Development of characterization techniques with liquefied gas solvents should also be developed further in order to gain more thorough understanding of the working mechanisms. As primary next steps, work could be done through Raman to help to understand the difference in phases when phase separation in electrolytes occurs. The polarizable molecular dynamics simulations could also be utilized to guide surface-based density functional theory calculations to better understand the decomposition of the electrolytes into SEI and CEI layers. Given the large size of aggregates, and large equilibration time of the ionicity seen in simulating electrolytes, advanced computing techniques (such a machine learned adaptive basis sets) could be utilized to increase the screening throughput for potentially effective electrolyte combinations.

Finally, researchers should try to make use of the unique features of the liquefied gas electrolytes. One potential path forward is the relative ease of recovery of the electrolyte when compared with liquid electrolytes. Given the high volatility of the electrolyte, there is significant possibility for the extraction and recycling of the electrolyte. Finally, given the good electrochemical stability of many of the liquefied gas solvents, as well as their highly fluorinated nature, it is likely that the electrolytes could be designed, and used, for alternative electrodes such as sulfur, oxygen, various catholytes, and anodes such as sodium.

The importance of multi-scale and multi-disciplinary development in the push towards a cleaner energy future cannot be overstated. This thesis demonstrates the use of this approach and will help future researchers to approach and understand energy storage-based issues in a similar manner.

REFERENCES

1. CO_2 and Greenhouse Gas Emissions - Our World in Data. https://ourworldindata.org/co2-and-other-greenhouse-gas-emissions#1-5-c-emissions-pathways.

2. Energy - Our World in Data. https://ourworldindata.org/energy.

3. A Degree of Concern: Why Global Temperatures Matter – Climate Change: Vital Signs of the Planet. https://climate.nasa.gov/news/2865/a-degree-of-concern-why-global-temperatures-matter/.

4. Battery Market Size Worth $310.8 Billion By 2027. https://www.grandviewresearch.com/press-release/global-battery-market.

5. Market Research Reports & Consulting | Grand View Research, Inc. https://www.grandviewresearch.com/.

6. Energy and environmental goals drive change.

7. Posada, J. O. G., Rennie, A. J. R., Villar, S. P., Martins, V. L., Marinaccio, J., Barnes, A., Glover, C. F., Worsley, D. A. & Hall, P. J. Aqueous batteries as grid scale energy storage solutions. *Renewable and Sustainable Energy Reviews* vol. 68 1174–1182 (2017).

8. Which is better for electric vehicles performance, LiFePO4 or ternary lithium-ion?-industry-news | Large Power. https://www.large.net/news/68u43n2.html.

9. Goodenough, J. B. & Gao, H. A perspective on the Li-ion battery. *Cit. Sci. CHINA Chem.* **62**, 1555 (2019).

10. Goodenough, J. B. & Kim, Y. Challenges for Rechargeable Li Batteries †. *Chem. Mater.* **22**, 587–603 (2010).

11. Xu, K. Nonaqueous Liquid Electrolytes for Lithium-Based Rechargeable Batteries. (2004) doi:10.1021/cr030203g.

12. Aurbach, D., Markovsky, B., Salitra, G., Markevich, E., Talyossef, Y., Koltypin, M., Nazar, L., Ellis, B. & Kovacheva, D. Review on electrode-electrolyte solution interactions, related to cathode materials for Li-ion batteries. *J. Power Sources* **165**, 491–499 (2007).

13. Liu, J., Bao, Z., Cui, Y., Dufek, E. J., Goodenough, J. B., Khalifah, P., Li, Q., Liaw, B. Y., Liu, P., Manthiram, A., Meng, Y. S., Subramanian, V. R., Toney, M. F., Viswanathan, V. V., Whittingham, M. S., Xiao, J., Xu, W., Yang, J., Yang, X.-Q., Zhang, J. -G. Pathways for practical high-energy long-cycling lithium metal batteries. *Nat. Energy* **4**, 180–186 (2019).

14. Mauger, A., Armand, M., Julien, C. M. & Zaghib, K. Challenges and issues facing lithium metal for solid-state rechargeable batteries. *J. Power Sources* **353**, 333–342 (2017).

15. Adar, F. *PERSPECTIVES ON THE HISTORY OF THE RAMAN EFFECT AND ITS*

IMPLEMENTATION. https://pubs.geoscienceworld.org/msa/elements/article-pdf/16/2/82/5013269/gselements-16-2-82.pdf (2020).

16. Young, A. T. Rayleigh scattering. *Appl. Opt.* **20**, 533 (1981).

17. DCM(75-09-2) Raman. https://www.chemicalbook.com/SpectrumEN_75-09-2_Raman.htm.

18. Han, S.-D., Borodin, O., Seo, D. M., Zhou, Z.-B. & Henderson, W. A. Electrolyte Solvation and Ionic Association. *J. Electrochem. Soc.* **161**, A2042–A2053 (2014).

19. Schindler, W., Zerda, T. W. & Jonas, J. High pressure Raman study of intermolecular interactions and Fermi resonance in liquid ethylene carbonate. *J. Chem. Phys.* **81**, 4306–4313 (1984).

20. Allen, M. P. Introduction to Molecular Dynamics Simulation. *Comput. Soft Matter* **23**, 1–28 (2004).

21. *Basics of Molecular Dynamics Simulation*.

22. Bedrov, D., Piquemal, J.-P., Borodin, O., MacKerell, A. D., Roux, B. & Schröder, C. Molecular Dynamics Simulations of Ionic Liquids and Electrolytes Using Polarizable Force Fields. *Chem. Rev.* acs.chemrev.8b00763 (2019) doi:10.1021/acs.chemrev.8b00763.

23. Borodin, O. Polarizable Force Field Development and Molecular Dynamics Simulations of Ionic Liquids. *J. Phys. Chem. B* **113**, 11463–11478 (2009).

24. Oleg Borodin*, † and & Grant D. Smith†, ‡. Development of Many−Body Polarizable Force Fields for Li-Battery Components: 1. Ether, Alkane, and Carbonate-Based Solvents. (2006) doi:10.1021/JP055079E.

25. Eyer, J. & Corey, G. *Energy Storage for the Electricity Grid: Benefits and Market Potential Assessment Guide A Study for the DOE Energy Storage Systems Program*. https://www.sandia.gov/ess-ssl/publications/SAND2010-0815.pdf (2010).

26. Walawalkar, R., Apt, J. & Mancini, R. Economics of electric energy storage for energy arbitrage and regulation in New York. *Energy Policy* **35**, 2558–2568 (2007).

27. Sioshansi, R., Denholm, P., Jenkin, T. & Weiss, J. Estimating the value of electricity storage in PJM: Arbitrage and some welfare effects. *Energy Econ.* **31**, 269–277 (2009).

28. Figueiredo, F. C., Flynn, P. C. & Cabral, E. A. The Economics of Energy Storage in 14 Deregulated Power Markets. *Energy Stud. Rev.* **14**, (2006).

29. Byrne, R. H., Concepcion, R. J. & Silva-Monroy, C. A. Estimating potential revenue from electrical energy storage in PJM. in *2016 IEEE Power and Energy Society General Meeting (PESGM)* 1–5 (IEEE, 2016). doi:10.1109/PESGM.2016.7741915.

30. Fitzgerald, G., Mandel, J., Morris, J. & Touati, H. *The Economics of Battery Energy Storage: how multi-use, customer-sted batteries deliver the most services and value to customers and the grid*. (2015).

31. Conover, D., Ferreira, S., Crawford, A., Schoenwald, D., Fuller, J., Rosewater, D., Gourisetti, S. & Viswanathan, V. *Protocol for Uniformly Measuring and Expressing the Performance of Energy Storage Systems*. https://energymaterials.pnnl.gov/pdf/PNNL-22010Rev2.pdf (2016).

32. Tenergy. Specification Approval Sheet - Lithium iron phosphate Battery. http://www.all-battery.com/datasheet/30067_datasheet.pdf (2014).

33. Tenergy. Specification Approval Sheet - Lithium-Ion Rechargeable Battery. http://www.tenergy.com/30001_datasheet.pdf (2010).

34. Tenergy. Specification Approval Sheet - Nickle Cadmium Battery. 12,13 http://www.tenergy.com/20203_datasheet.pdf (2012).

35. EnerSys. Cyclon Batteries. http://www.enersys.com/Cyclon_Batteries.aspx?langType=1033 (2008).

36. Alveo Energy. http://www.alveoenergy.com/.

37. Leadbetter, J. & Swan, L. G. Selection of battery technology to support grid-integrated renewable electricity. *J. Power Sources* **216**, 376–386 (2012).

38. Akhil, A. A., Huff, G., Currier, A., Kaun, B., Rastler, D., Chen, S. B., Cotter, A., Bradshaw, D. & Gauntlett, W. *DOE/EPRI Electricity Storage Handbook in Collaboration with NRECA*. hhttps://prod.sandia.gov/techlib-noauth/access-control.cgi/2015/151002.pdf (2015).

39. Batteries, H. O. F., Library, D. E. & Companies, T. M. Handbook of batteries. *Cell* 1200 (2004) doi:10.1016/0378-7753(86)80059-3.

40. Byrne, R. H., Donnelly, M. K., Loose, V. W. & Trudnowski, J. D. Methodology to Determine the Technical Performance and Value Proposition for Grid-Scale Energy Storage Systems. SAND2012-10639 (2012).

41. Bolun Xu, Dvorkin, Y., Kirschen, D. S., Silva-Monroy, C. A. & Watson, J.-P. A comparison of policies on the participation of storage in U.S. frequency regulation markets. in *2016 IEEE Power and Energy Society General Meeting (PESGM)* 1–5 (IEEE, 2016). doi:10.1109/PESGM.2016.7741531.

42. CAISO. *Flexible Ramping Product*. https://www.caiso.com/Documents/DraftTechnicalAppendix_FlexibleRampingProduct.pdf (2015).

43. Dunn, B., Kamath, H., Tarascon, J.-M., Soloveichik, G. L., Winter, M., Brodd, R. J.,

Simon, P., Gogotsi, Y., Goodenough, J. B., Kim, Y., Tarascon, J. M., Armand, M., Etacheri, V., Marom, R., Elazari, R., Salitra, G., Aurbach, D., Armand, M., Tarascon, J. M., Aricò, A. S., Bruce, P., Scrosati, B. ,Tarascon, J. M., Schalkwijk, W. van, Li, H., Wang, Z. X., Chen, L. Q., Huang, X. J., Poizot, P., Laruelle, S., Grugeon, S., Dupont, L., Tarascon, J. M., Obrovac, M. N., Christensen, L., Barpanda, P., Yamada, A., Chung, S. C., Hinokuma, K., Tarascon, J. M., Tarascon, J. M., Chen, H., Girishkumar, G., McCloskey, B., Luntz, A. C., Swanson, S., Wilcke, W., Lee, K. T., Abraham, K. M., Jiang, Z., Zheng, J. P., Liang, R. Y., Hendrickson, M., Plichta, E. J., Ogasawara, T., Débart, A., Holzapfel, M., Novák, P., Bruce, P. G., Débart, A., Paterson, A. J., Bao, J., Bruce, P. G., Lu, Y. C., Girishkumar, G., McCloskey, B., Luntz, A. C., Swanson, S., Wilcke, W., Whitacre, J. F., Tevar, A., Sharma, S., Yao, Y. F. Y., Kummer, J. T., Lu, X. C., Xia, G. G., Lemmon, J. P., Yang, Z., G., Dustmann, C. H., Farrington, G. C., Briant, J. L., Rosa, D. La, Sudworth, J. L., Yang, Z., Song, S. F., Dunn, B., Breiter, M. W., Park, D. S., Leon, C. P. de, Bartolozzi, M., Skyllas-Kazacos, M., Rychcik, M., Robins, R. G., Fane, A. G., Green, M. A., Skyllas-Kazacos, M., Doughty, D. H., Butler, P. C., Akhil, A. A., Clark, N. H., Boyes, J. D., Nguyen, T., Savinell, R. F., Duduta, M., Lu, Y. H., Goodenough, J. B.. Electrical energy storage for the grid: a battery of choices. *Science* **334**, 928–35 (2011).

44. Yang, Z., Zhang, J., Kintner-Meyer, M. C. W., Lu, X., Choi, D., Lemmon, J. P. & Liu, J. Electrochemical Energy Storage for Green Grid. *Chem. Rev.* **111**, 3577–3613 (2011).

45. Akhil, A., Zaininger, H., Hurtwitch, J. & Badin, J. *Battery Energy Storage: A Preliminary Assessment of National Benefits (The Gateway Benefits Study)*. https://www.osti.gov/servlets/purl/10116044 (1993).

46. Ragone, D. V. Review of Battery Systems for Electrically Powered Vehicles. 9 (1968) doi:10.4271/680453.

47. Joseph, A. & Shahidehpour, M. Battery storage systems in electric power systems. in *2006 IEEE Power Engineering Society General Meeting* 8 pp. (IEEE, 2006). doi:10.1109/PES.2006.1709235.

48. Byrne, R. H. & Silva-Monroy, A. *Estimating the Maximum Potential Revenue for Grid Connected Electricity Storage: Arbitrage and Regulation*. http://www.sandia.gov/ess/publications/SAND2012-3863.pdf (2012).

49. Xu, B., Dvorkin, Y., Kirschen, D. S., Silva-Monroy, C. A. & Watson, J.-P. A Comparison of Policies on the Participation of Storage in U.S. Frequency Regulation Markets. *IEEE PES Innov. Smart Grid Technol. Conf. Eur.* 16–20 (2016) doi:10.1109/PESGM.2016.7741531.

50. Nguyen, T. A., Byrne, R. H., Concepcion, R. J. & Gyuk, I. Maximizing revenue from electrical energy storage in MISO energy frequency regulation markets. in *2017 IEEE Power & Energy Society General Meeting* 1–5 (IEEE, 2017). doi:10.1109/PESGM.2017.8274348.

51. Luo, X., Wang, J., Dooner, M. & Clarke, J. Overview of current development in electrical energy storage technologies and the application potential in power system operation. *Appl.*

Energy **137**, 511–536 (2015).

52. Divya, K. C. & Østergaard, J. Battery energy storage technology for power systems—An overview. *Electr. Power Syst. Res.* **79**, 511–520 (2009).

53. MIZUSHIMA, K., JONES, P. C., WISEMAN, P. J. & GOODENOUGH, J. B. Lixcoo2 (O Less-Than X Less-Than-or-Equal-To 1) - a New Cathode Material for Batteries of High-Energy Density. *Solid State Ionics* **3**–**4**, 171–174 (1981).

54. Whittingham*, M. S. Lithium Batteries and Cathode Materials. (2004) doi:10.1021/CR020731C.

55. Turcheniuk, K., Bondarev, D., Singhal, V. & Yushin, G. Ten years left to redesign lithium-ion batteries. *Nature* **559**, 467–470 (2018).

56. Liu, B., Zhang, J.-G. & Xu, W. Advancing Lithium Metal Batteries. *Joule* **2**, 833–845 (2018).

57. Cheng, X.-B., Zhang, R., Zhao, C.-Z. & Zhang, Q. Toward Safe Lithium Metal Anode in Rechargeable Batteries: A Review. *Chem. Rev.* **117**, 10403–10473 (2017).

58. Xu, W., Wang, J., Ding, F., Chen, X., Nasybulin, E., Zhang, Y. & Zhang, J.-G. Lithium metal anodes for rechargeable batteries. *Energy Environ. Sci.* **7**, 513–537 (2014).

59. Ding, F., Xu, W., Chen, X., Zhang, J., Engelhard, M. H., Zhang, Y., Johnson, B. R., Crum, J. V, Blake, T. A., Liu, X. & Zhang, J.-G. Effects of Carbonate Solvents and Lithium Salts on Morphology and Coulombic Efficiency of Lithium Electrode. *J. Electrochem. Soc.* 160 (2013) doi:10.1149/2.100310jes.

60. Rustomji, C. S., Yang, Y., Kim, T. K., Mac, J., Kim, Y. J., Caldwell, E., Chung, H. & Meng, Y. S. Liquefied gas electrolytes for electrochemical energy storage devices. *Science* **356**, eaal4263 (2017).

61. Yang, Y., Yin, Y., Davies, D. M., Zhang, M., Mayer, M., Zhang, Y., Sablina, E. S., Wang, S., Lee, J. Z., Borodin, O., Rustomji, C. S. & Meng, Y. S. Liquefied gas electrolytes for wide-temperature lithium metal batteries. *Energy Environ. Sci.* **13**, 2209 (2020).

62. Suo, L., Xue, W., Gobet, M., Greenbaum, S. G., Wang, C., Chen, Y., Yang, W., Li, Y. & Li, J. Fluorine-donating electrolytes enable highly reversible 5-V-class Li metal batteries. *Proc. Natl. Acad. Sci. U. S. A.* **115**, 1156–1161 (2018).

63. Suo, L., Borodin, O., Gao, T., Olguin, M., Ho, J., Fan, X., Luo, C., Wang, C. & Xu, K. 'Water-in-salt' electrolyte enables high-voltage aqueous lithium-ion chemistries. *Science (80-.).* **350**, (2015).

64. Wu, F., Chu, F., Ferrero, G. A., Sevilla, M., Fuertes, A. B., Borodin, O., Yu, Y. & Yushin, G. Boosting High-Performance in Lithium-Sulfur Batteries via Dilute Electrolyte. *Nano Lett.* **20**, 5391–5399 (2020).

65. Borodin, O., Giffin, G. A., Moretti, A., Haskins, J. B., Lawson, J. W., Henderson, W. A. & Passerini, S. Insights into the Structure and Transport of the Lithium, Sodium, Magnesium, and Zinc Bis(trifluoromethansulfonyl)imide Salts in Ionic Liquids. *J. Phys. Chem. C* **122**, 20108–20121 (2018).

66. Castillo, E. C. Standards for electric vehicle batteries and associated testing procedures. *Adv. Batter. Technol. Electr. Veh.* 469–494 (2015) doi:10.1016/B978-1-78242-377-5.00018-2.

67. Zhao, R., Liu, J. & Gu, J. A comprehensive study on Li-ion battery nail penetrations and the possible solutions. *Energy* **123**, 392–401 (2017).

68. Mao, B., Chen, H., Cui, Z., Wu, T. & Wang, Q. Failure mechanism of the lithium ion battery during nail penetration. *Int. J. Heat Mass Transf.* **122**, 1103–1115 (2018).

69. Davies, D., Rustomji, C. S., Yang, Y., Lee, J. & Meng, Y. S. Electrochemical cell cap. (2020).

70. NIST WebBook. https://webbook.nist.gov/.

71. Yangyuchen Yang , Daniel M. Davies , Yijie Yin , Oleg Borodin, Jungwoo Lee , Chengcheng Fang , Marco Olguin , Xuefeng Wang, Yihui Zhang , Katya Sablina , Cyrus . Rustomji, Y. S. M. High Efficiency Lithium Metal Anode Enabled by Liquefied Gas Electrolytes. *Joule* (2019).

72. ASHRAE. *Designation and Safety Classification of Refrigerants*. https://www.ashrae.org/File Library/Technical Resources/Standards and Guidelines/Standards Addenda/34_2016_g_20180628.pdf (2018).

73. ISO - ISO 817:2014 - Refrigerants — Designation and safety classification. https://www.iso.org/standard/52433.html.

74. Takizawa, K., Takahashi, A., Tokuhashi, K., Kondo, S. & Sekiya, A. Burning velocity measurement of HFC-41, HFC-152, and HFC-161 by the spherical-vessel method. *J. Fluor. Chem.* **127**, 1547–1553 (2006).

75. Domanski, P. A., McLinden, M. O., Bell, I. H. & Linteris, G. T. *Low-GWP alternative refrigerant blends for HFC-134a*. https://nvlpubs.nist.gov/nistpubs/TechnicalNotes/NIST.TN.2014.pdf (2018) doi:10.6028/NIST.TN.2014.

76. Hu, L., Montzka, S. A., Lehman, S. J., Godwin, D. S., Miller, B. R., Andrews, A. E., Thoning, K., Miller, J. B., Sweeney, C., Siso, C., Elkins, J. W., Hall, B. D., Mondeel, D. J., Nance, D., Nehrkorn, T., Mountain, M., Fischer, M. L., Biraud, S. C., Chen, H., Tans, P. P. Considerable contribution of the Montreal Protocol to declining greenhouse gas emissions from the United States. *Geophys. Res. Lett.* **44**, 8075–8083 (2017).

77. AHRI Air-conditioning, heating, & refrigeration institute. *Risk Assessment of*

Refrigeration Systems Using A2L Flammable Refrigerants. http://www.ahrinet.org/App_Content/ahri/files/RESEARCH/Technical Results/AHRI-8009_Final_Report.pdf.

78. Calm, J. . & Hourahan, G. C. Physical, Safety, and Environmental Data For Current and Alternative Refrigerants. *Refrig. Sustain. Dev.* (2011).

79. Wilson, D. P. & Richard, R. G. Determination of refrigerant lower flammability limits in compliance with proposed addendum p to standard 34. *ASHRAE Trans.* **108**, 739–755.

80. Hess, S., Wohlfahrt-Mehrens, M. & Wachtler, M. Flammability of Li-Ion Battery Electrolytes: Flash Point and Self-Extinguishing Time Measurements. *J. Electrochem. Soc.* **162**, A3084–A3097 (2015).

81. Rustomji, C. S., Yang, Y., Kim, T. K., Mac, J., Kim, Y. J., Caldwell, E., Chung, H. & Meng, Y. S. Liquefied gas electrolytes for electrochemical energy storage devices. *Science* **356**, eaal4263 (2017).

82. Hagos, T. T., Thirumalraj, B., Huang, C.-J., Abrha, L. H., Hagos, T. M., Berhe, G. B., Bezabh, H. K., Cherng, J., Chiu, S.-F., Su, W.-N. & Hwang, B.-J. Locally Concentrated LiPF6 in Carbonate-based Electrolyte with Fluoroethylene Carbonate as a Diluent for Anode-Free Lithium Metal Battery. *ACS Appl. Mater. Interfaces* acsami.8b21052 (2019) doi:10.1021/acsami.8b21052.

83. Ren, X., Zou, L., Jiao, S., Mei, D., Engelhard, M. H., Li, Q., Lee, H., Niu, C., Adams, B. D., Wang, C., Liu, J., Zhang, J.-G. & Xu, W. High-Concentration Ether Electrolytes for Stable High-Voltage Lithium Metal Batteries. *ACS Energy Lett.* 896–902 (2019) doi:10.1021/acsenergylett.9b00381.

84. Nikolay Goutev, *, Keiichi Ohno, and & Matsuura, H. Raman Spectroscopic Study on the Conformation of 1,2-Dimethoxyethane in the Liquid Phase and in Aqueous Solutions. (2000) doi:10.1021/JP001340+.

85. Brouillette, D., Irish, D. E., Taylor, N. J., Perron, G., Odziemkowski, M. & Desnoyers, J. E. Stable solvates in solution of lithium bis(trifluoromethylsulfone)imide in glymes and other aprotic solvents: Phase diagrams, crystallography and Raman spectroscopyElectronic supplementary information (ESI) available: Crystallographic data (single crystal data) in cif format (CCDC reference number 184345). See http://www.rsc.org/suppdata/cp/b2/b203776a/. *Phys. Chem. Chem. Phys.* **4**, 6063–6071 (2002).

86. Seo, D. M., Borodin, O., Balogh, D., O'Connell, M., Ly, Q., Han, S.-D., Passerini, S. & Henderson, W. A. Electrolyte Solvation and Ionic Association III. Acetonitrile-Lithium Salt Mixtures–Transport Properties. *J. Electrochem. Soc.* **160**, A1061–A1070 (2013).